

DTIC FILE COPY

(2)

MEMORANDUM REPORT BRL-MR-3873

BRL

AD-A229 113

TEMPERATURE HISTORIES OF
SMALL METALLIC FRAGMENTS
TRAPPED IN PROPELLING CHARGES

MARTIN S. MILLER

OCTOBER 1990

DTIC
ELECTE
NOV 08 1990
S B D

APPROVED FOR PUBLIC RELEASE; DISTRIBUTION UNLIMITED.

U.S. ARMY LABORATORY COMMAND

BALLISTIC RESEARCH LABORATORY
ABERDEEN PROVING GROUND, MARYLAND

90 11 8 106

NOTICES

Destroy this report when it is no longer needed. DO NOT return it to the originator.

Additional copies of this report may be obtained from the National Technical Information Service, U.S. Department of Commerce, 5285 Port Royal Road, Springfield, VA 22161.

The findings of this report are not to be construed as an official Department of the Army position, unless so designated by other authorized documents.

The use of trade names or manufacturers' names in this report does not constitute indorsement of any commercial product.

UNCLASSIFIED

REPORT DOCUMENTATION PAGE			Form Approved OMB No. 0704-0188	
<small>Public reporting burden for this collection of information is estimated to average 1 hour per response, including the time for reviewing instructions, searching existing data sources, gathering and maintaining the data needed, and completing and reviewing the collection of information. Send comments regarding this burden estimate or any other aspect of this collection of information, including suggestions for reducing this burden, to Washington Headquarters Services, Directorate for Information Operations and Reports, 1215 Jefferson Davis Highway, Suite 1204, Arlington, VA 22202-4302, and to the Office of Management and Budget, Paperwork Reduction Project (0704-0188), Washington, DC 20503.</small>				
1. AGENCY USE ONLY (Leave blank)		2. REPORT DATE October 1990		3. REPORT TYPE AND DATES COVERED Final 1 Jun 90 - 31 Jul 90
4. TITLE AND SUBTITLE TEMPERATURE HISTORIES OF SMALL METALLIC FRAGMENTS TRAPPED IN PROPELLING CHARGES			5. FUNDING NUMBERS 1L162618A1FL ✓	
6. AUTHOR(S) Martin S. Miller				
7. PERFORMING ORGANIZATION NAME(S) AND ADDRESS(ES)			8. PERFORMING ORGANIZATION REPORT NUMBER	
9. SPONSORING / MONITORING AGENCY NAME(S) AND ADDRESS(ES) U.S. Army Ballistic Research Laboratory ATTN: SLCBR-DD-T Aberdeen Proving Ground, MD 21005-5066			10. SPONSORING / MONITORING AGENCY REPORT NUMBER BRL-MR-3873	
11. SUPPLEMENTARY NOTES				
12a. DISTRIBUTION / AVAILABILITY STATEMENT Approved for public release; distribution unlimited			12b. DISTRIBUTION CODE	
13. ABSTRACT (Maximum 200 words) <p>Small metallic fragments can be trapped in combustible cartridge cases during manufacture and released into the interior-ballistic flow upon combustion of the case. Such particles may survive the interior-ballistic cycle and pose an ignition threat to the case of the next round or to unburned combustion gases mixing with air as the breech is opened. In this report the particle temperature is computed at the time of projectile exit, making use of the one-dimensional code IBHVG2 to characterize the interior-ballistic flow. The fragment is assumed to be released at the instant of case burnout and its trajectory along the flow streamline computed approximately in order to quantify the heat-transfer rate. Uncertainties in particle drag are treated by examining maximum, average, and minimum values. Aluminum and steel fragments are considered and temperature histories computed as a function of fragment mass, shape, and initial axial location. It is found that, for fragments imbedded in the outer-radius of the combustible case, only very small fragment sizes completely vaporize. Fragments initially located near the breech are ones most likely to remain in the gun chamber after firing and these particles can achieve temperatures in excess of 2000°C. A complete assessment of the ignition threat posed by these fragments will require the development of experiments to test the susceptibility of combustible-case materials to fragments of combined size and temperature similar to those computed in this report.</p>				
14. SUBJECT TERMS Fragments, Metal, Propelling Charges, Temperature, Guns			15. NUMBER OF PAGES	
			16. PRICE CODE	
17. SECURITY CLASSIFICATION OF REPORT Unclassified	18. SECURITY CLASSIFICATION OF THIS PAGE Unclassified	19. SECURITY CLASSIFICATION OF ABSTRACT Unclassified	20. LIMITATION OF ABSTRACT UL	

NSN 7540-01-280-550C

UNCLASSIFIED

Standard Form 298 (Rev 2-89)
Prescribed by ANSI Std Z39-18
298-102

INTENTIONALLY LEFT BLANK.

TABLE OF CONTENTS

	<u>PAGE</u>
LIST OF FIGURES	v
1. INTRODUCTION	1
2. BASIC ASSUMPTIONS	1
3. CONSERVATION EQUATION GOVERNING THE FRAGMENT TEMPERATURE	2
4. RATE OF HEAT TRANSFER TO THE FRAGMENT	3
4.1 HEAT TRANSFER COEFFICIENTS	4
4.2 COMPUTATION OF FLOW CONDITIONS AT THE FRAGMENT	5
4.3 EQUATION OF MOTION OF THE FRAGMENT	5
4.4 BOUNDS ON THE HEAT TRANSFER	9
5. RADIATIVE HEAT TRANSFER VS. CONVECTIVE HEAT TRANSFER ...	13
6. RESULTS AND DISCUSSION	13
7. CONCLUSIONS	21
REFERENCES	41
APPENDICES	43
LIST OF SYMBOLS	57
DISTRIBUTION LIST	59



BY	
Distribution/	
Availability Codes	
Dist	Avail and/or Special
A-1	

INTENTIONALLY LEFT BLANK

LIST OF FIGURES

<u>FIGURE</u>	<u>PAGE</u>
1. Schematic illustrating relationship between variables	6
2. Plot of the integrand in Eq. 22	8
3. Upper and lower bounds on v_{gf} after injection near breech	10
4. Upper and lower bounds on v_{gf} after injection at chamber midlength	11
5. Upper and lower bounds on v_{gf} after injection at case mouth	12
6. Comparison of radiative to conductive heat transfer	14
7. Temperature history of aluminum fragment ($s = .3$ cm, $d = .03$ cm) originating at the case mouth	15
8. Temperature history of steel fragment ($s = .3$ cm, $d = .03$ cm) originating at the case mouth	16
9. Temperature history of aluminum fragment ($s = .3$ cm, $d = .03$ cm) originating at case midlength	17
10. Temperature history of steel fragment ($s = .3$ cm, $d = .03$ cm) originating at case midlength	18
11. Temperature history of aluminum fragment ($s = .3$ cm, $d = .03$ cm) originating near the breech	19
12. Temperature history of steel fragment ($s = .3$ cm, $d = .03$ cm) originating near the breech	20
13. Temperature history of aluminum fragment ($s = .6$ cm, $d = .03$ cm) originating at case mouth	22
14. Temperature history of steel fragment ($s = .6$ mm, $d = .03$ mm) originating at the case mouth	23
15. Temperature history of aluminum fragment ($s = .6$ mm, $d = .03$ mm) originating near the breech	24
16. Temperature history of steel fragment ($s = .6$ cm, $d = .03$ cm) originating near the breech	25

17.	Temperature history of aluminum fragment ($s = .15$ cm, $d = .03$ cm) originating at the case mouth	26
18.	Temperature history of steel fragment ($s = .15$ cm, $d = .03$ cm) originating at the case mouth	27
19.	Temperature history of aluminum fragment ($s = .15$ cm, $d = .03$ cm) originating near the breech	28
20.	Temperature history of steel fragment ($s = .15$ cm, $d = .03$ cm) originating near the breech	29
21.	Temperature history of aluminum fragment ($s = .3$ cm, $d = .02$ cm) originating at case mouth	30
22.	Temperature history of steel fragment ($s = .3$ mm, $d = .02$ mm) originating at the case mouth	31
23.	Temperature history of aluminum fragment ($s = .3$ mm, $d = .02$ mm) originating at case midlength	32
24.	Temperature history of steel fragment ($s = .3$ cm, $d = .02$ cm) originating at case midlength	33
25.	Temperature history of aluminum fragment ($s = .3$ cm, $d = .02$ cm) originating near the breech	34
26.	Temperature history of steel fragment ($s = .3$ cm, $d = .02$ cm) originating near the breech	35
27.	Temperature history of aluminum fragment ($s = .05$ cm, $d = .0025$ cm) originating at the case mouth	36
28.	Temperature history of steel fragment ($s = .05$ cm, $d = .0025$ cm) originating at the case mouth	37
29.	Temperature history of aluminum fragment ($s = .05$ cm, $d = .0025$ cm) originating at the breech	38
30.	Temperature history of steel fragment ($s = .05$ cm, $d = .0025$ cm) originating at the breech	39

1. Introduction

Metallic fragments occasionally are found imbedded in combustible cartridge cases as a result of manufacturing anomalies. During the interior-ballistic cycle, these particles are released into the interior flow field as the case is consumed. Components of the propelling charge, such as igniters, may also be a source of metallic fragments during normal functioning. A concern of system designers is that these fragments may not be ejected from the gun or vaporized and pose an ignition threat either to subsequently loaded cases or to fuel-rich combustion gases mixing with air upon opening of the breech. This report is a first effort to quantify the temperature history of such particles in a 120 mm tank cannon as a function of their mass, shape, composition, and initial location. It should be noted that, while the fragment temperature history is prerequisite to establishing the seriousness of the ignition threat for a given set of circumstances, experiments to establish the ignitability of combustible case material or combustion gases are required to complete the assessment.

The objective of the work documented in this report was to formulate the problem mathematically and to solve it using a level of approximation expedient to gaining an appreciation of the various factors involved, given a one-month time constraint. The analysis shows that the fragment temperature is critically dependent upon the description of the particle drag, which for a tumbling wafer-like geometry is difficult to assess. This uncertainty is handled by computing upper and lower bounds on the drag and determining how these bounds map into the solution for the temperature history. Analytical approximations to the equations are utilized, and no doubt the temperature histories could be improved by solving the equations numerically. It is believed, however, that the uncertainties in the particle drag overshadow inaccuracies introduced by the mathematical approximations.

2. Basic Assumptions

1. Fragments are thin wafers such that the surface area associated with their edges is negligible compared with that of their faces. This geometry is expected and simplifies the mathematics but the assumption could readily be removed if desired. In addition, the fragments are assumed to be square wafers for convenience.
2. The particles are not in thermal contact with the gun-tube wall. Presumably, a small fragment would be kept in motion by turbulence and would experience only brief and occasional contact with the wall.
3. Time for intra-fragment thermal relaxation is short compared to the rate of heat transfer to the fragment (due to the high thermal diffusivity of metal); therefore, no temperature gradients exist in the fragment.
4. Radiation heat transfer between the gas and the particles is negligible. (This is shown to be a valid approximation.)

5. The interior-ballistic flow is adequately characterized by the IBHVG2 code. Since the time interval of interest is after flamespreading is complete, this lumped-parameter code should give a reasonable first-order description of the flow. An assumption which is uncertain, however, is that the case burns uniformly along its length. Erosive effects could increase the rate of surface regression at the case mouth (i.e., projectile end of case), however, tests with inert cases show no such preferential erosion.. On the other hand, the pressure, which in the code is independent of distance, in reality is higher at the breech and this fact tends to increase the rate of burning at the breech. To some unknown extent, these effects compensate for each other.

6. Combustion of the fragments is not considered. Presumably, combustion would increase the rate of consumption and heating of the particle, so that here an upper bound to the survival time of the fragment is computed.

3. Conservation Equation Governing the Fragment Temperature

If τ is the time after injection of the fragment into the flow, (other symbols are identified in the List of Symbols)

$$\rho Vc \frac{dT}{d\tau} = Ah(T_{gf} - T) + \epsilon \sigma A(T_{gf}^4 - T^4) \quad (1)$$

Neglecting radiation heat transfer (for the moment), and assuming T_{gf} is constant,

$$\rho Vc \frac{dT}{d\tau} = Ah(T_{gf} - T) \quad (2)$$

Changing variables to $\Theta = T_{gf} - T$ and considering h constant,

$$\frac{d\Theta}{d\tau} = -\frac{Ah}{\rho Vc} \Theta = -\frac{2h}{\rho dc} \Theta \quad (3)$$

Assuming $T = T_0$ at $\tau = 0$ ($T_0 = 300$ K throughout this report.)

$$T_{gf} - T = (T_{gf} - T_0) e^{-\frac{2h}{\rho dc} \tau} \quad (4)$$

$$T(\tau) = T_{gf} - (T_{gf} - T_0)e^{-\frac{2h}{\rho dc}\tau} \quad (5)$$

This equation will govern the temperature rise of the fragment up to the melting point, requiring a time $\Delta\tau_1$ given by

$$\Delta\tau_1 = \frac{\rho dc}{2h} \ln \left(\frac{T_{gf} - T_0}{T_{gf} - T_m} \right) \quad (6)$$

at the end of which time the temperature will remain constant until the heat of fusion is delivered to the fragment. This requires a period of time $\Delta\tau_m$ given by

$$\Delta\tau_m = \frac{\rho d \Delta H_{fusion}}{2h(T_{gf} - T_m)} \quad (7)$$

When melting is complete, the melted mass (assuming it remains intact, has the same shape, density, and heat capacity) resumes its temperature rise according to

$$T(\tau) = T_{gf} - (T_{gf} - T_m)e^{-\frac{2h}{\rho dc}\tau} \quad (8)$$

for a time interval $\Delta\tau_2$ given by

$$\Delta\tau_2 = \frac{\rho dc}{2h} \ln \left(\frac{T_{gf} - T_m}{T_{gf} - T_b} \right) \quad (9)$$

When the boiling point is reached, the temperature of the molten fragment again remains constant for a time $\Delta\tau_{vap}$ until the heat of vaporization is delivered.

$$\Delta\tau_{vap} = \frac{\rho d \Delta H_{vap}}{2h(T_{gf} - T_b)} \quad (10)$$

At the end of this period the fragment is completely vaporized.

4. Rate of Heat Transfer to the Fragment

The heart of the fragment heating problem is in the computation of the heat transfer coefficient. This necessitates an empirical correlation function, given in the next section, and

a calculation of the relative velocity between the accelerating fragment and the gas flow, which is itself a function of time and position.

4.1 Heat Transfer Coefficients

Case 1: Static Gas

Melvin¹ determined a heat transfer coefficient for a metal sphere in a static gas. For a sphere of radius a

$$h = \frac{\lambda}{a} \quad (11)$$

Defining an equivalent radius of the fragment wafer as the radius of a sphere of same surface area as the fragment,

$$a = \sqrt{\frac{A}{4\pi}} \quad (12)$$

Case 2: Moving Gas

The heat transfer coefficient used in the NOVA interior-ballistic code is due to Gelperin and Ainstein². This correlation is for spheres. Its use for non-spherical particles of equivalent area, though common, has not been tested.

$$Nu = 1 + 0.2Re^{0.67}Pr^{0.33} \quad (13)$$

where

$$Nu \equiv \frac{ah}{\lambda} \quad (14)$$

$$Re \equiv \frac{2\rho_g va}{\mu} \quad (15)$$

where v is the velocity of the flow relative to the fragment.

$$Pr \equiv \frac{c_p \mu}{\lambda} \quad (16)$$

Eqs. 13 and 14 reduce to Eq. 11 in the limit of zero flow velocity.

4.2 Computation of Flow Conditions at the Fragment

The fragment location in the cartridge case most likely to result in the fragment's survival is the outside surface of the case in contact with the chamber wall. All calculations will be based on this radial location though different axial locations will be considered. Thus the fragment is considered to be "injected" into the interior-ballistic flow at the time of burnout of the combustible case. In order to compute the temperature history of the fragment, one must estimate the velocity of the combustion gases relative to that of the fragment, $(v_{gf} - v_f)$. In order to determine this velocity, one must compute the trajectory of the fragment along the flow streamline. This calculation proceeds as follows. (Fig. 1 may be helpful in visualizing the variables at the time of injection, t_i , and at the time of projectile exit, t_e .)

4.3 Equation of Motion of the Fragment

The velocity of the fragment, v_f , with mass m is obtained by solving its equation of motion:

$$m \frac{dv_f}{d\tau} = C_D \frac{1}{2} \rho_g (v_{gf} - v_f)^2 A_s \quad (17)$$

where C_D is the drag coefficient of the fragment, $\rho_g (v_{gf} - v_f)^2 / 2$ is the free-stream dynamic pressure on the fragment, and A_s is the sectional fragment area presented to the flow. For constant v_{gf} the fragment equation of motion can be solved analytically to give

$$v_f(\tau) = \frac{\beta v_{gf}^2 \tau}{1 + \beta v_{gf} \tau} \quad (18)$$

where β is defined by

$$\beta = \frac{C_D \rho_g A_s}{2m} \quad (19)$$

Note that C_D has been assumed constant in Eq. 17 but that it often is a function of the Reynolds number, particularly at the transition from laminar to turbulent flow. The maximum drag on the fragment occurs when the normal to the fragment surface is oriented in the direction of the flow. The value of the drag coefficient under this condition is approximately 1. In orientations where the surface normal is perpendicular to the flow, the drag will assume a very low value due to the small edge area presented. One could average the drag over all possible orientations under the assumption that the particle is tumbling; however, for purposes of this limited analysis, it is deemed preferable to compute bounds on the behavior to avoid making unwarranted assumptions. The maximum value of β is therefore computed using a $C_D = 1$ and $A_s = s^2$, whereas the minimum value of β assumes

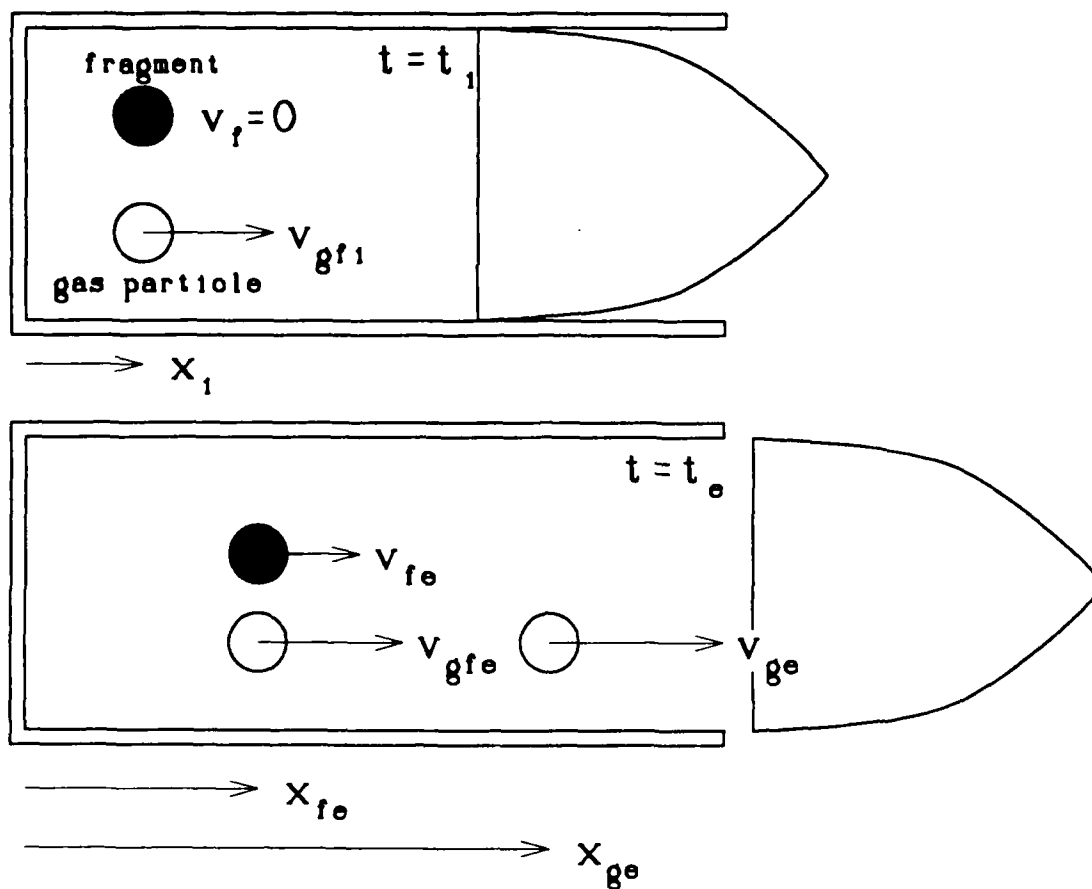


Fig. 1. Schematic illustrating relationship between variables

$C_D = 1$ and $A_s = sd$. Although the minimum value of C_D would be less than 1, the very small edge area should provide an effective lower bound on β .

Integrating v_f from Eq. 18 over τ , one gets for the position of the fragment x_f

$$x_f(\tau) = x_i + v_{gf}\tau - \frac{\ln(1 + \beta v_{gf}\tau)}{\beta} \quad (20)$$

The approximation that v_{gf} is constant in the fragment equation of motion will now be examined. The velocity of the combustion gases (more precisely, the two-phase combusting fluid), v_g , at any time and position behind the projectile is given by

$$v_g(x, t) = \frac{xv_p(t)}{L_c + \xi_p(t)} \quad (21)$$

where x is the distance from the breech block, $v_p(t)$ is the projectile velocity at time t , L_c is the length of the chamber, and $\xi_p(t)$ is the distance traveled by the projectile at time t . This linear velocity profile is consistent with the assumptions of the computer code³ (IBHVG2) used to characterize the interior ballistic conditions. The time τ is referenced to the time of combustible-case burnout, i.e., the fragment is injected at $\tau = 0$, or t_i . The motion of a fluid particle originating at the position x_i and time of injection, is obtained by integrating Eq. 21 as follows:

$$\int_{x_i}^{x_f} \frac{dx}{x} = \int_0^{\tau} \frac{v_p(\tau' + t_i)}{L_c + \xi_p(\tau' + t_i)} d\tau' \quad (22)$$

The integrand on the right side of this equation is shown in Fig. 2 plotted as a function of gun time t . Case burnout occurs at $t_i = 3.85$ ms, so the integrand is well approximated as a linear function for times longer than 3.85 ms. Thus, for $\tau > 0$, based on a simple two-point fit,

$$\frac{v_p}{L_c + \xi_p} = 587 - 1.12 \times 10^5 \tau \quad (s^{-1}) \quad (23)$$

Using Eq. 23 in Eq. 22, the position of the fluid particle at time τ is given by

$$x_g(\tau) = x_i e^{587\tau - 5.6 \times 10^4 \tau^2} \quad (24)$$

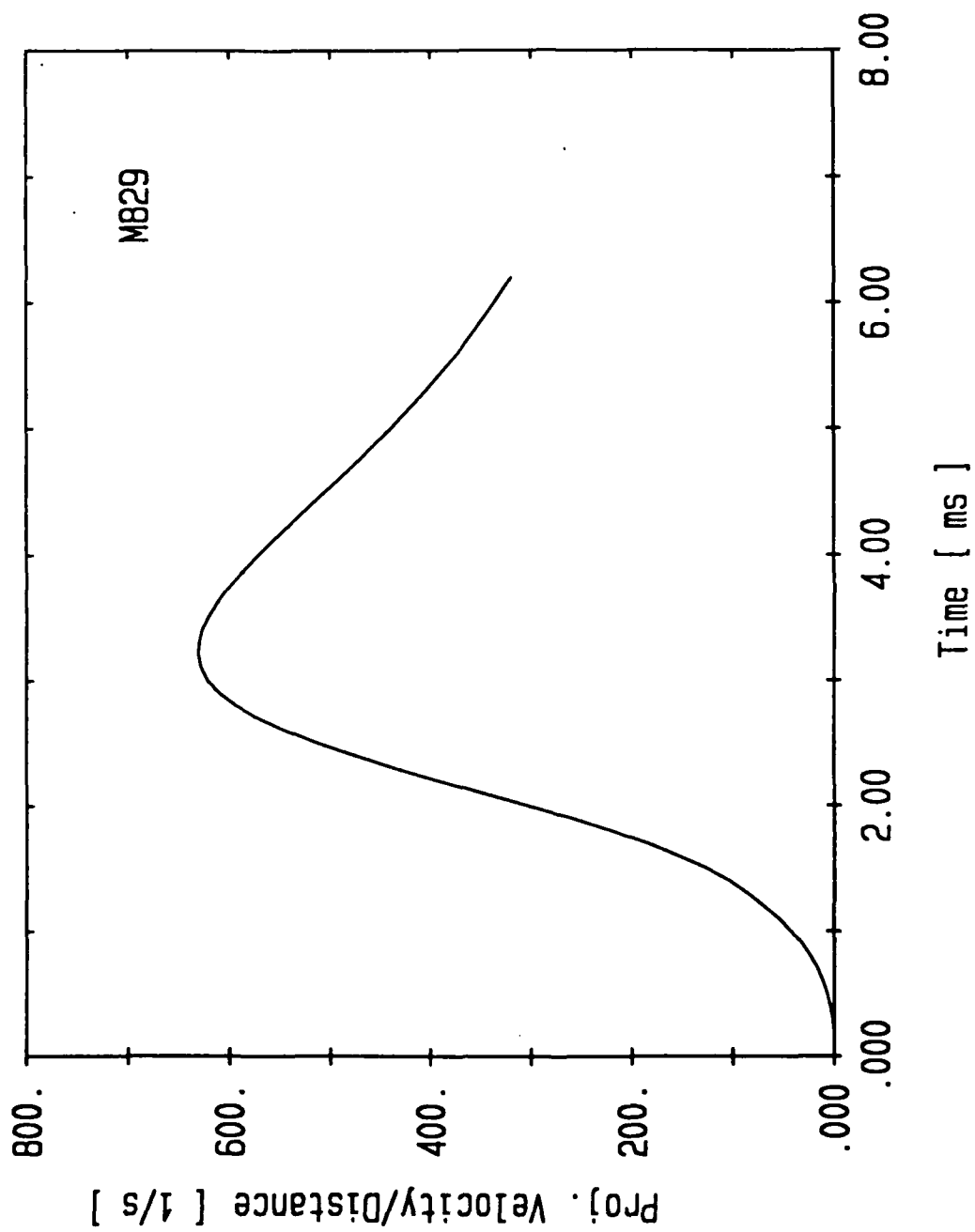


Fig. 2. Plot of the integrand in Eq. 22

Eqs. 18 and 20 were derived on the assumption of constant v_{gf} . We now discuss how to choose a suitable value for purposes of this analysis. Since, at a given time, the gas velocity is a linear function of position, a lower bound on the velocity of the gas in contact with the fragment can be found by using x_i in Eq. 21. Since the fragment can never completely catch up with the fluid particle which passes it at the instant of injection, an upper limit on v_{gf} can be constructed by using Eq. 24 in Eq. 21. Thus, upper and lower bounds on v_{gf} as a function of time can be readily computed and are shown in Figs. 3 - 5 for three axial injection positions. The heat transfer to the fragment is very sensitive to injection position near the breech face because IBHVG2 assumes that the velocity is zero at the breech wall. In reality even minor turbulence will sweep the fragment from the breech wall. To reflect this behavior, we have arbitrarily taken 1 cm as the minimum distance from the breech to be considered here. Calculations assuming that v_{gf} is constant at the injection value v_{gfi} , i.e., v_g at x_i and $\tau = 0$, can be used to calculate (using Eq. 20) x_f at projectile exit time, τ_e , and this distance can in turn be used in Eq. 21 to estimate v_{gf} at projectile exit time. We label this value, v_{gfe} , and print out the value for every run. In the cases thus far examined v_{gfe} is within 30 % of v_{gfi} in almost all cases and always within 37 %. The accuracy of the computations could, of course, be improved by numerically integrating the coupled, non-linear differential equations describing the system, but in our judgement this error is by far overshadowed by the uncertainty in the drag on the fragment.

4.4 Bounds on the Heat Transfer

In order to compute the heat transfer from the flow to the fragment after injection, the velocity of the gas in contact with the fragment relative to the velocity of the fragment is required, i.e., v in Eq. 15, where

$$v = v_{gf} - v_f \quad (25)$$

We will compute the average value of v in the interval $(0, \tau_e)$ as follows:

$$\langle v \rangle = \langle v_{gf} - v_f \rangle = \langle v_{gf} \rangle - \langle v_f \rangle = \frac{1}{\tau_e} \int_0^{\tau_e} v_{gf} d\tau - \frac{1}{\tau_e} \int_0^{\tau_e} v_f d\tau \quad (26)$$

$$\langle v \rangle = v_{gfi} - \frac{x_f(\tau_e)}{\tau_e} \quad (27)$$

v_{gf} in Eq. 26 is taken as v_{gfi} to be consistent with the assumptions of the fragment-trajectory calculation. In those cases where v_{gf} increases appreciably over the time interval $(0, \tau)$ v_f should also increase, tending to minimize changes in v .

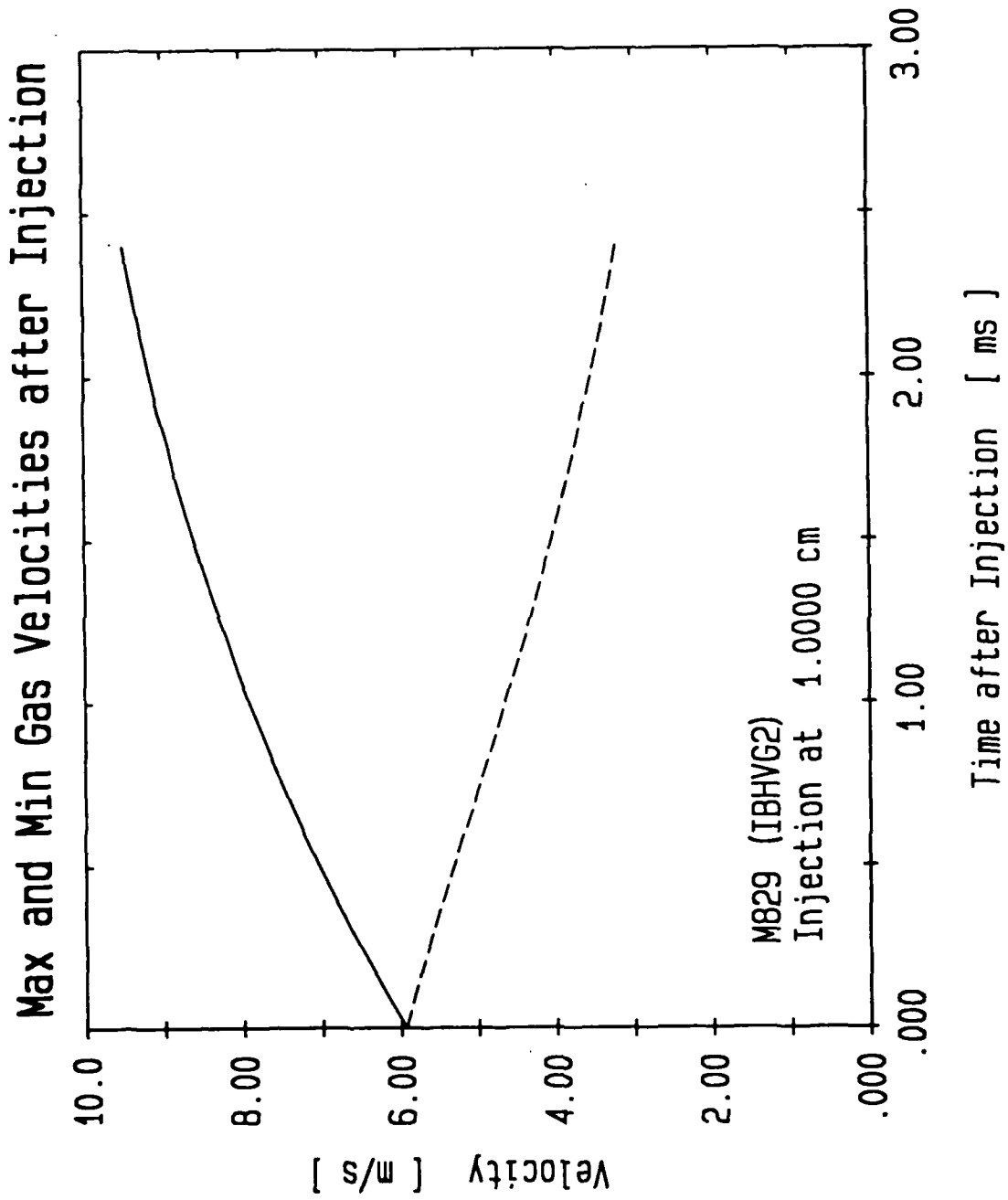


Fig. 3. Upper and lower bounds on v_g after injection near breech

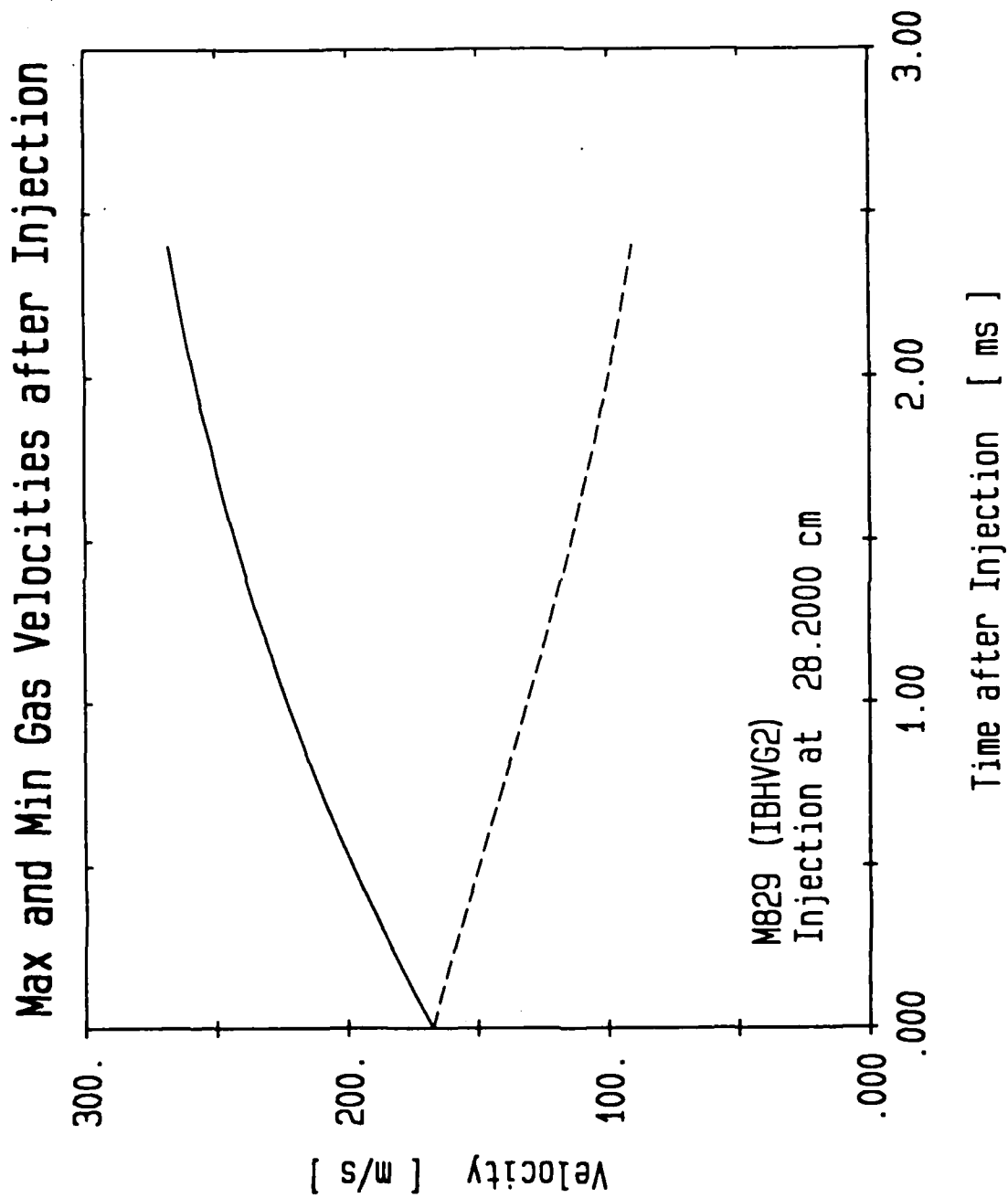


Fig. 4. Upper and lower bounds on v_d after injection at chamber midlength

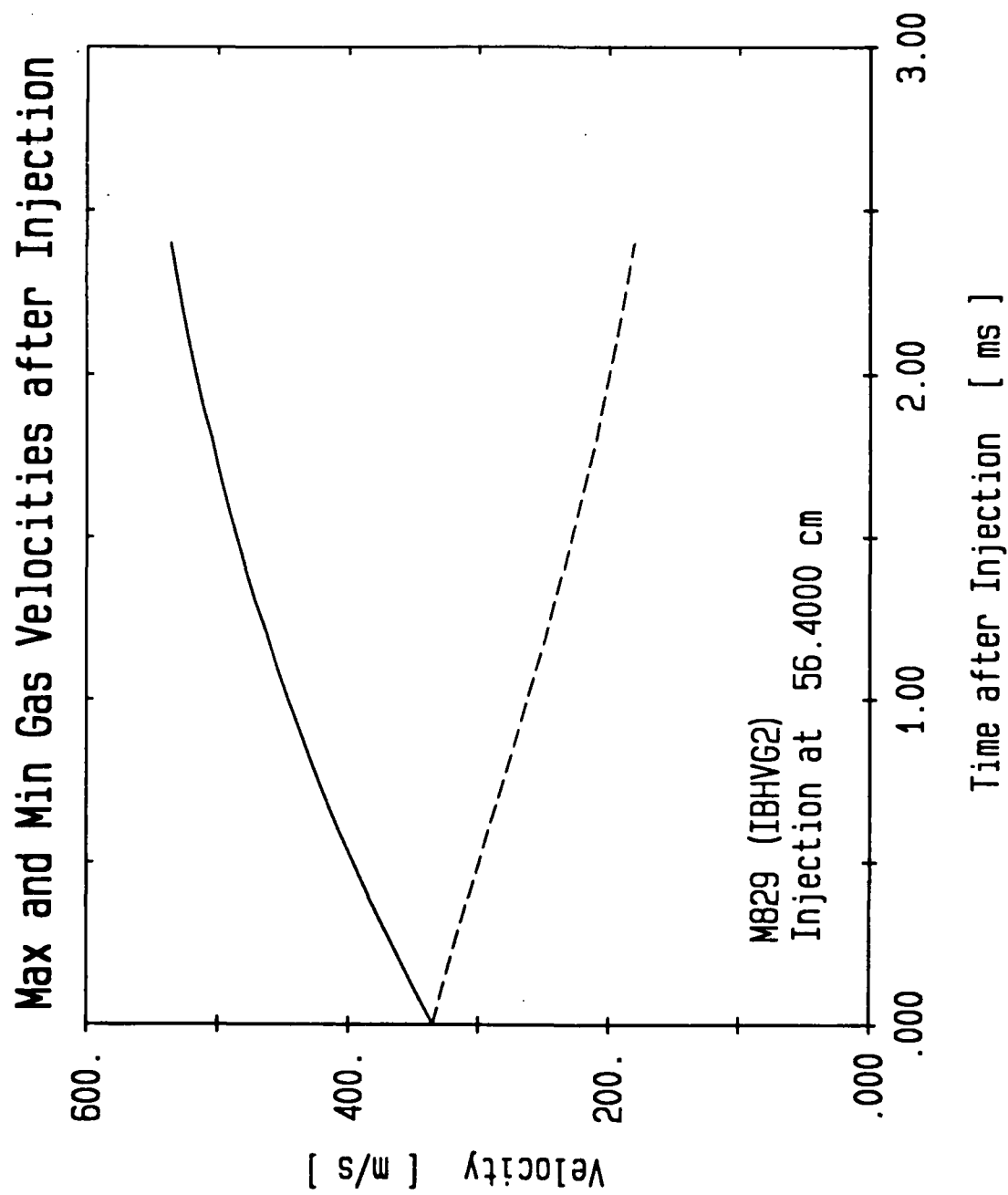


Fig. 5. Upper and lower bounds on v_g after injection at case mouth

Since the derivations of Eqs. 5 - 10 assumed constant T_{gf} , we may maximize the heat transfer by choosing as T_{gf} the maximum value of the flow temperature T_g in the interval $(0, \tau_e)$, using the minimum drag constant β for x_f in Eq. 20. Similarly, the minimum value of T_g may be used for T_{gf} , coupled with the maximum β , to obtain the minimum heat transfer. The arithmetic average of these two extreme temperatures is used in conjunction with the arithmetic average value of β in the "average" temperature histories shown in the figures. It should be pointed out that use of the average relative velocity in Eq. 26, in a strict sense, invalidates the temperature history details computed by Eq. 2. In reality, the relative velocity at early times is much higher than $\langle v \rangle$ and at late times much lower. However, the computed value of fragment temperature at projectile exit time should be valid, since the $\langle v_f \rangle$ in Eq. 27 is the average value which properly takes into account the non-linear time dependence of v_f given by Eq. 18.

5. Radiative Heat Transfer vs. Convective Heat Transfer

Radiative heat transfer can be shown to be negligible compared to that by convection by examining the case of minimum convective transfer, i.e., at an injection position near the breech. In Fig. 6 the fragment thermal history determined by Eq. 2 is used to compute the relative magnitude of these two heat transfer mechanisms. The radiative transfer is dwarfed by convection even under the minimum convection conditions. This justifies Eq. 2 as an excellent approximation.

6. Results and Discussion

All of the results thus far computed pertain to the M829 round. Figs. 7 - 12 show the temperature histories of a square fragment 0.3 cm on a side by 0.03 cm thick. Figs. 7 and 8 assume the fragment (aluminum and steel, respectively) is located initially at the case mouth. Figs. 9 and 10 assume the fragment is initially at the midlength of the case, and Figs. 11 and 12 take the initial fragment location as 1 cm from the breech wall. Clearly, the assumptions relating to the drag on the fragment have a very strong effect on the computed results, particularly at the case mouth. If the drag is high, then the fragment quickly accommodates to the velocity of the flow and the convective heat transfer is minimized. The volumetric heat capacity of steel is about 28 % higher than aluminum over the temperature range considered. Therefore, for equal heating rates the temperature of the steel is lower than that of the aluminum. However, the mass of the steel fragment is higher, leading to a lower acceleration, and therefore higher relative velocity between the fragment and the flow. This tends to increase the heat transfer to the steel fragment, in opposition to the heat-capacity effect. For the most part, the increased heat-transfer effect dominates, leading to higher temperatures for the steel fragment. Exceptions to this pattern are often found near the breech, however (e.g., Figs. 11 and 12). Here the fragment velocity is a small

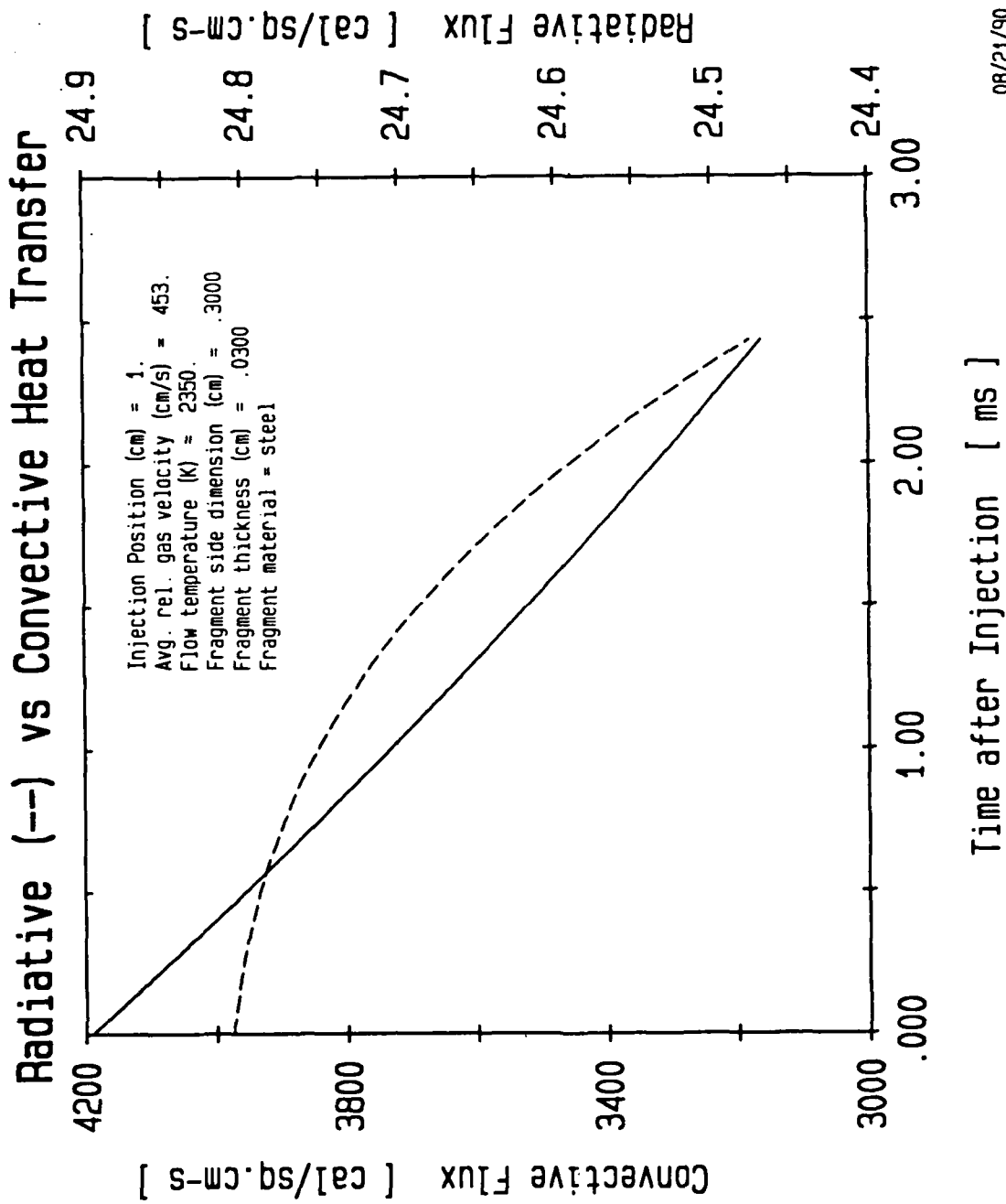


Fig. 6. Comparison of radiative to conductive heat transfer

M829 : Fragment at Case Mouth

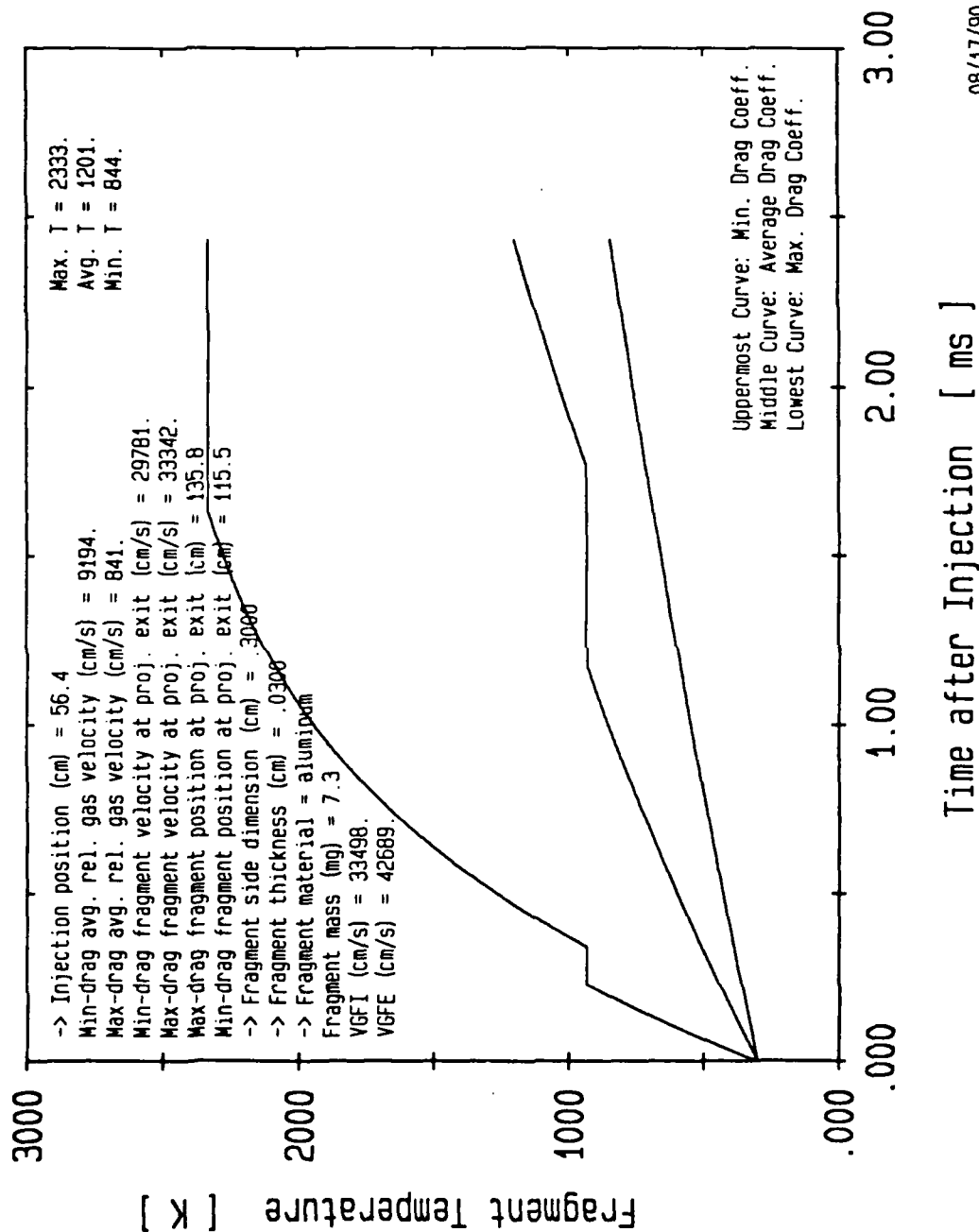


Fig. 7. Temperature history of aluminum fragment (s = .3 cm, d = .03 cm) originating at the case mouth

08/17/90

-> Injection position (cm) = 56.4
 Min-drag avg. rel. gas velocity (cm/s) = 16061.
 Max-drag avg. rel. gas velocity (cm/s) = 1959.
 Min-drag fragment velocity at proj. exit (cm/s) = 24602.
 Max-drag fragment velocity at proj. exit (cm/s) = 33051.
 Max-drag fragment position at proj. exit (cm) = 133.0
 Min-drag fragment position at proj. exit (cm) = 98.8
 -> Fragment side dimension (cm) = .3000
 -> Fragment thickness (cm) = .0300
 -> Fragment material = steel
 Fragment mass (mg) = 21.2
 VGFI (cm/s) = 33498.
 VGFE (cm/s) = 41835.

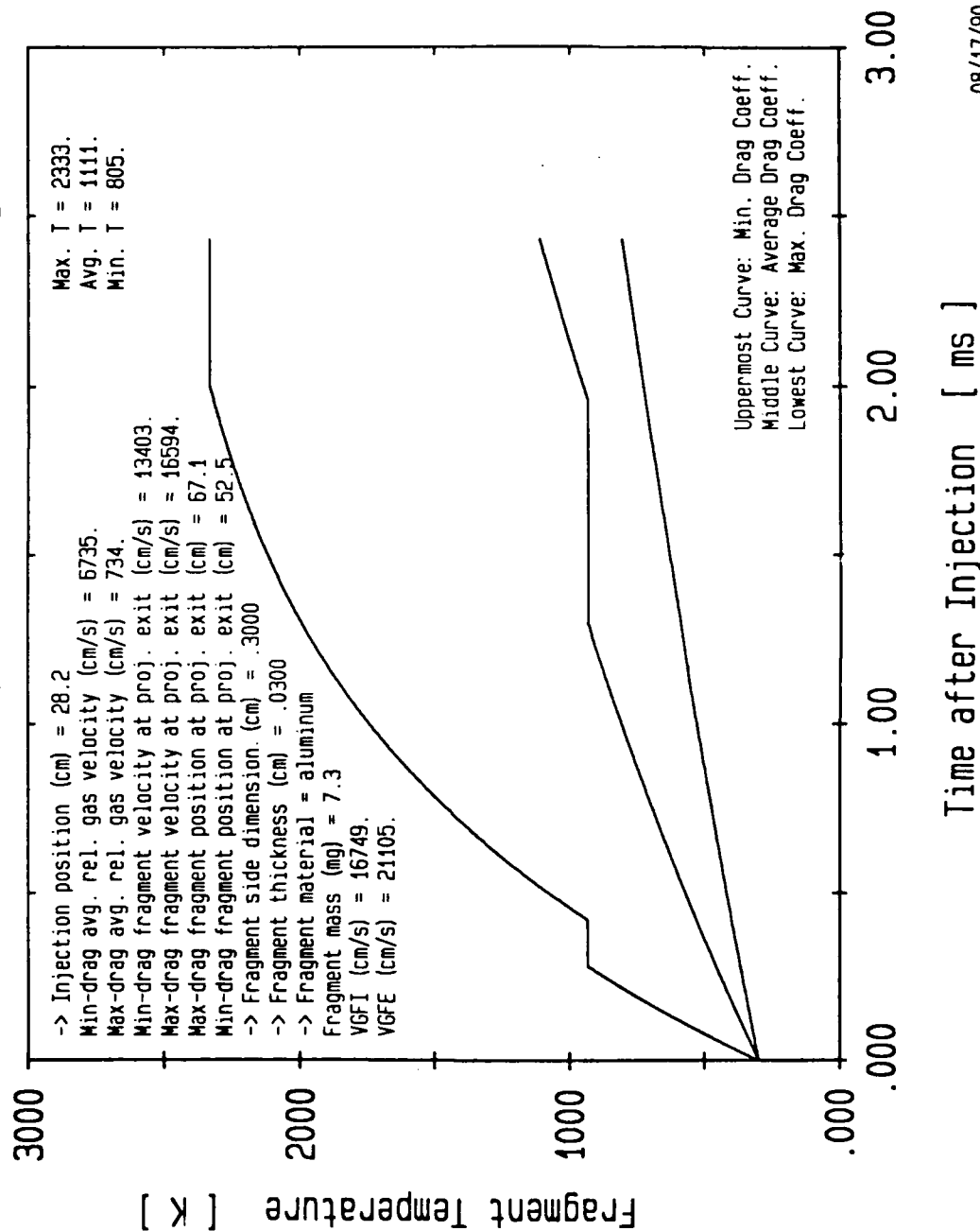
Max. $T = 2529$.
 Avg. $T = 1617$.
 Min. $T = 999$.

Uppermost Curve: Min. Drag Coeff.
 Middle Curve: Average Drag Coeff.
 Lowest Curve: Max. Drag Coeff.

08/17/90

Fig. 8. Temperature history of steel fragment ($s = .3$ cm, $d = .03$ cm) originating at the case mouth

M829 : Fragment at Case Midlength



08/17/90

Fig. 9. Temperature history of aluminum fragment ($s = .3$ cm, $d = .03$ cm) originating at case midlength

MB29 : Fragment at Case Midlength

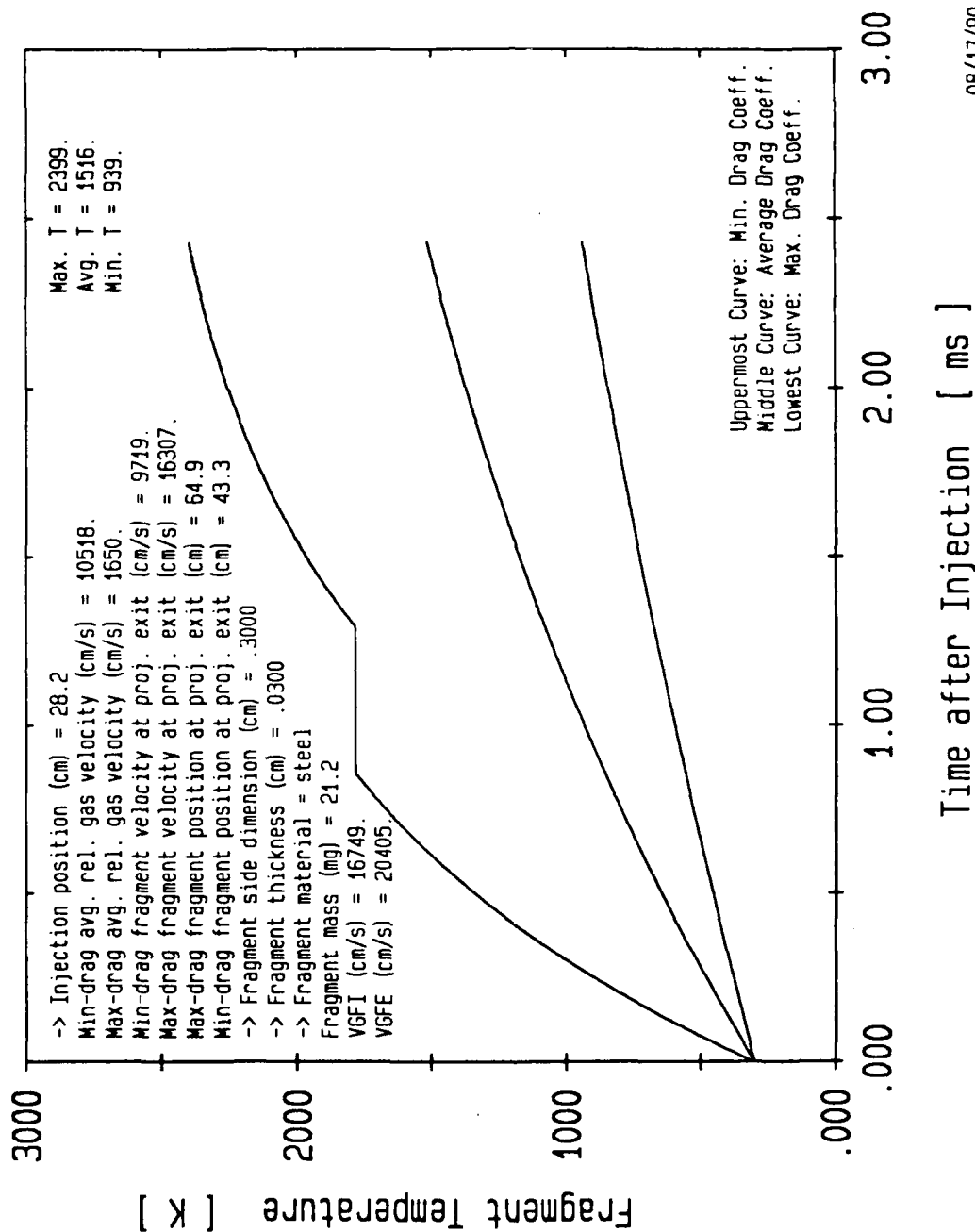
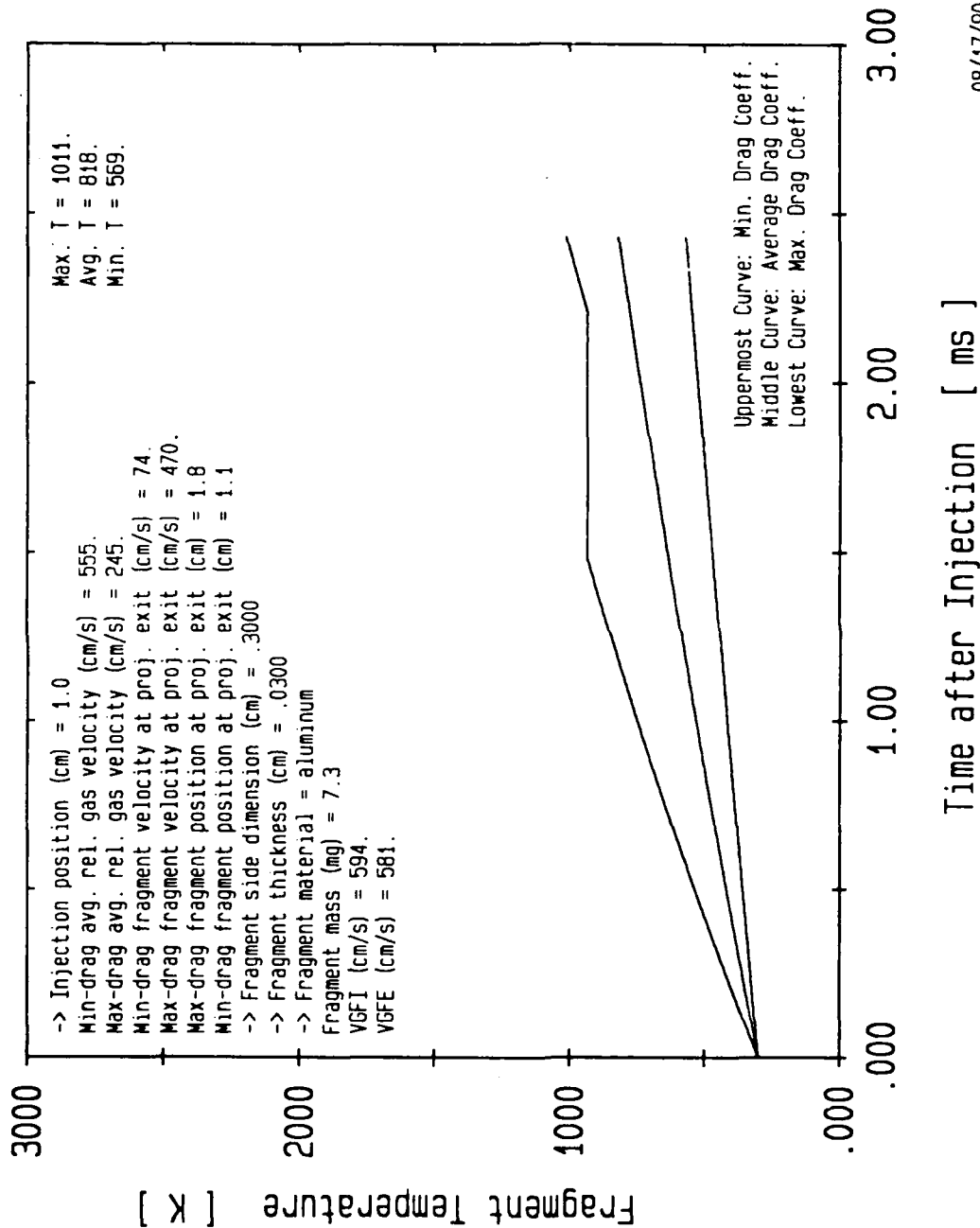


Fig. 10. Temperature history of steel fragment (s = .3 cm, d = .03 cm) originating at case midlength

M829 : Fragment near Breech



08/17/90

Fig. 11. Temperature history of aluminum fragment ($s = .3$ cm, $d = .03$ cm) originating near the breech

M829 : Fragment near Breach

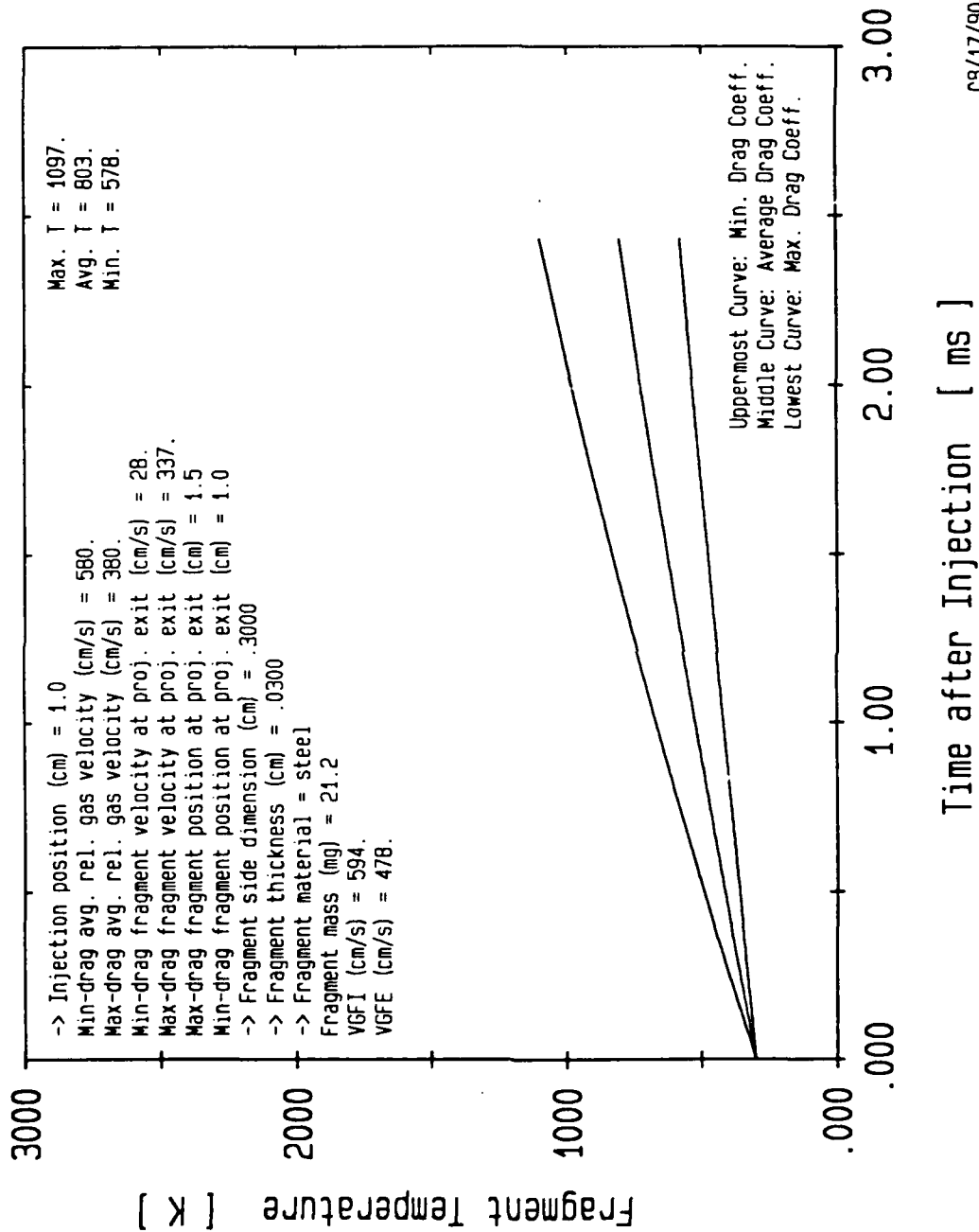


Fig. 12. Temperature history of steel fragment ($s = .3$ cm, $d = .03$ cm) originating near the breach

09/17/90

fraction of the flow velocity for both aluminum and steel, minimizing the heat transfer effect and emphasizing the heat-capacity effect.

The effect of both increasing and decreasing the fragment side dimension by a factor of 2 is shown in Figs. 13 - 20. In general, the highest fragment temperatures are associated with case-mouth origins, but these fragments also achieve the highest forward velocities and therefore are likely to leave the gun tube after shot ejection. It is interesting to note, however, that in this series of runs the fragment position at the time of projectile exit never reaches more than 25 % of the combined barrel/chamber length (531 cm) because of the late time of injection during the IB cycle.

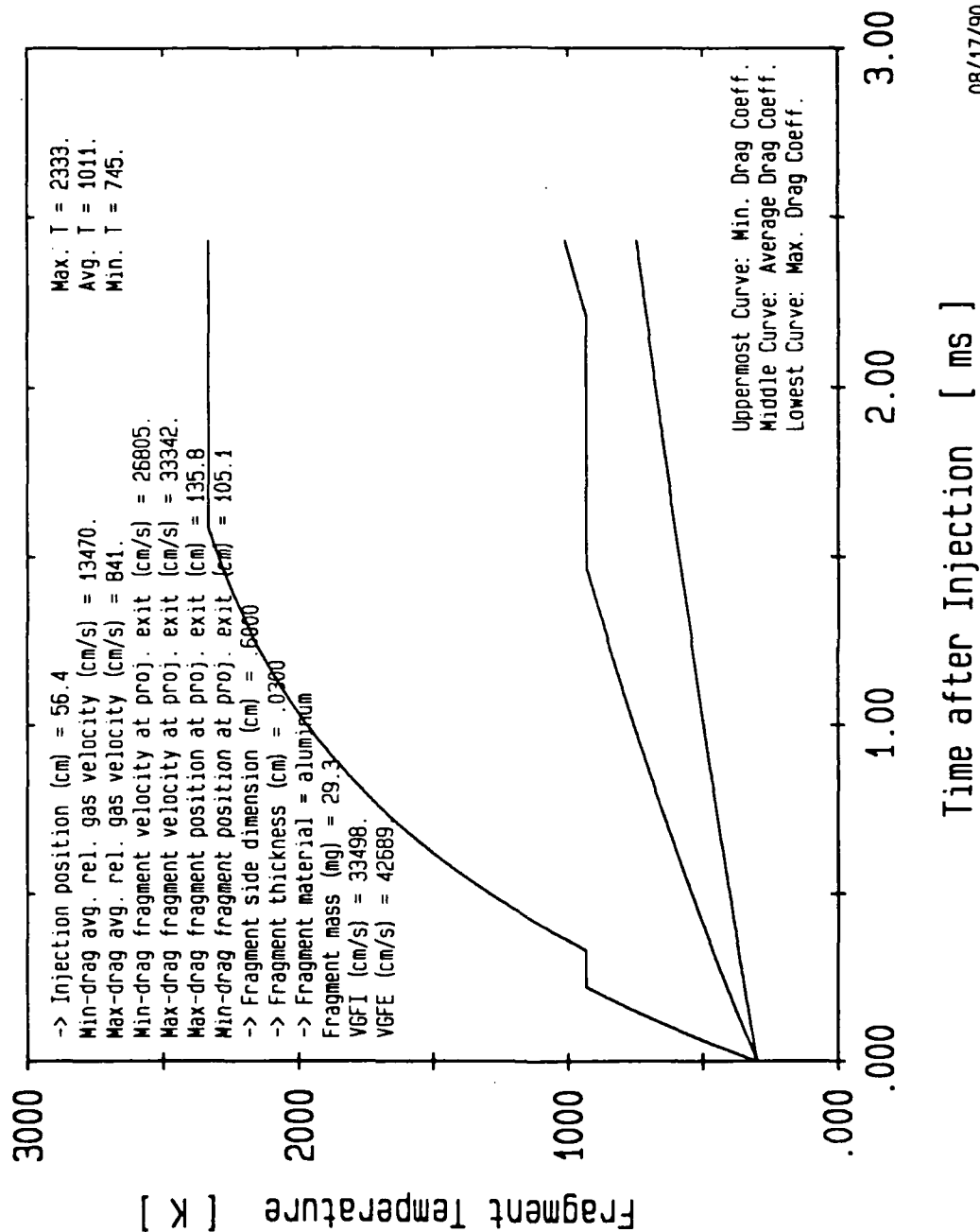
Decreasing the thickness of the 0.3 cm side fragment to 0.02 cm changes the thermal histories as shown in Figs. 21 - 26.

A set of fragment dimensions resulting in complete vaporization is found in Fig. 27. The fragment thickness here is 0.0025 cm (0.001 in.) and its side dimension is 0.05 cm (0.02 in.). This size is very close to the threshold of complete vaporization. (The dotted line ends at the time of complete conversion to vapor.) It clearly takes a relatively long time to supply the large (2720 cal/g) heat of vaporization. Under "average" assumptions in this same figure, the fragment has not quite begun to vaporize. Under the same conditions, a steel fragment (Fig. 28) stabilizes at the maximum flow temperatures in the molten state. Figs. 29 and 30 show the same size fragment originating near the breech. Note that velocities of these fragments, both aluminum and steel, are low but their temperatures are quite high and therefore may pose a serious ignition threat.

7. Conclusions

The problem of a metallic fragment, trapped in a combustible cartridge case, and heated by the combustion gases during the interior-ballistic cycle has been posed mathematically in this report. In order to compute the convective heat transfer from the combustion gases, one must compute the trajectory of the fragment along the flow streamline, then couple this information to the equation governing the internal energy of the fragment. An approximate solution to this problem has been constructed using analytic solutions valid under restricted conditions. A numerical solution to the set of coupled non-linear differential equations describing this system would eliminate the inaccuracies of the analytic approach used; however, in our judgement, the largest uncertainties in these calculations arise from uncertainties in the description of the drag of a wafer-like particle tumbling in the flow. In the calculations presented here, this uncertainty is treated by computing bounds on the thermal history of the fragment arising from bounds on the fragment drag. It could well be that the chaotic motion of fragments in the interior-ballistic flow would be characterized by large fluctuations about the mean behavior. If this is the case, placing bounds on the behavior is the most meaningful approach from an engineering-design perspective.

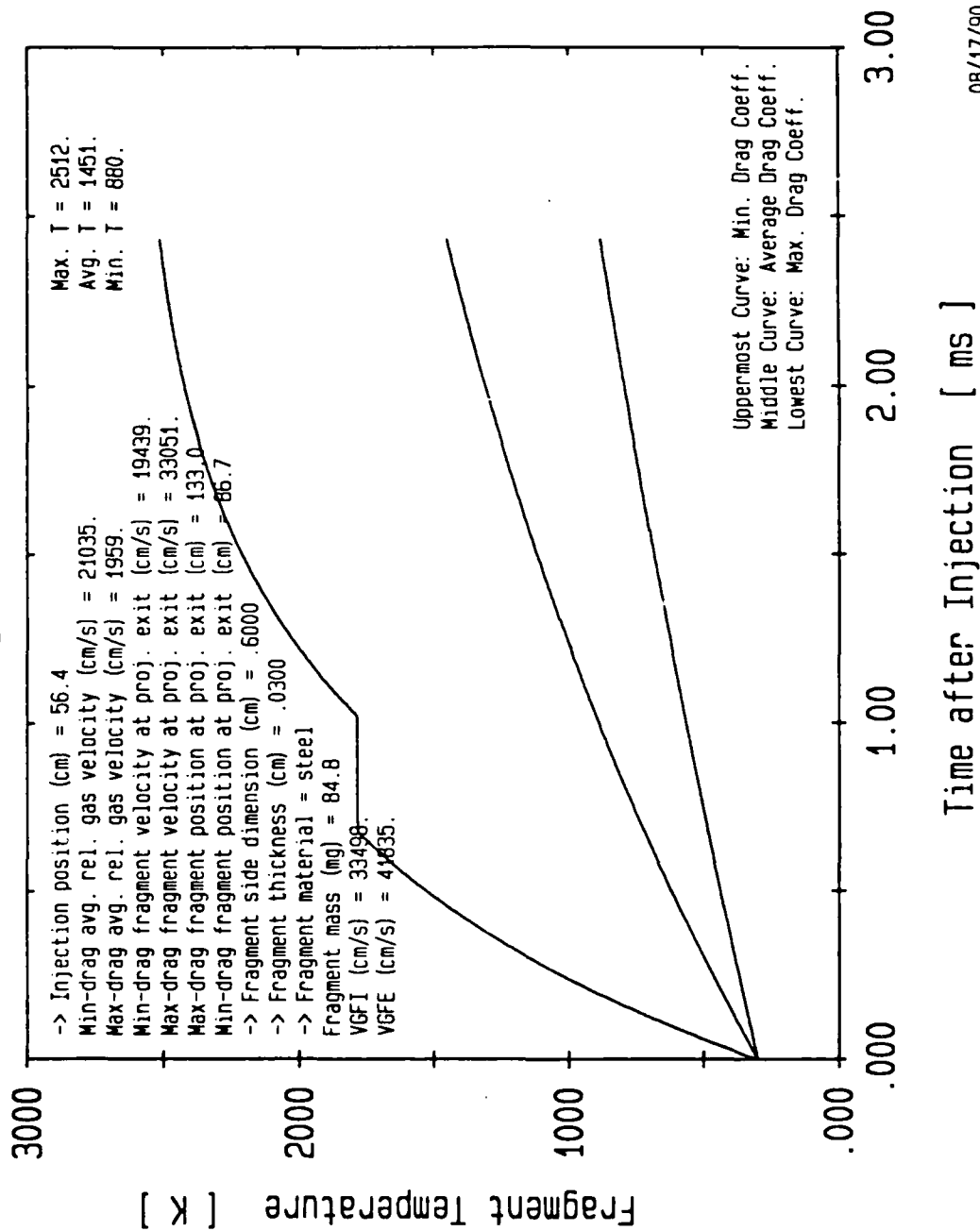
M829 : Fragment at Case Mouth



08/17/90

Fig. 13. Temperature history of aluminum fragment ($s = .6$ cm, $d = .03$ cm) originating at case mouth

M829 : Fragment at Case Mouth



08/17/90

Fig. 14. Temperature history of steel fragment ($s = .6$ mm, $d = .03$ mm) originating at the case mouth

MB29 : Fragment near Breech

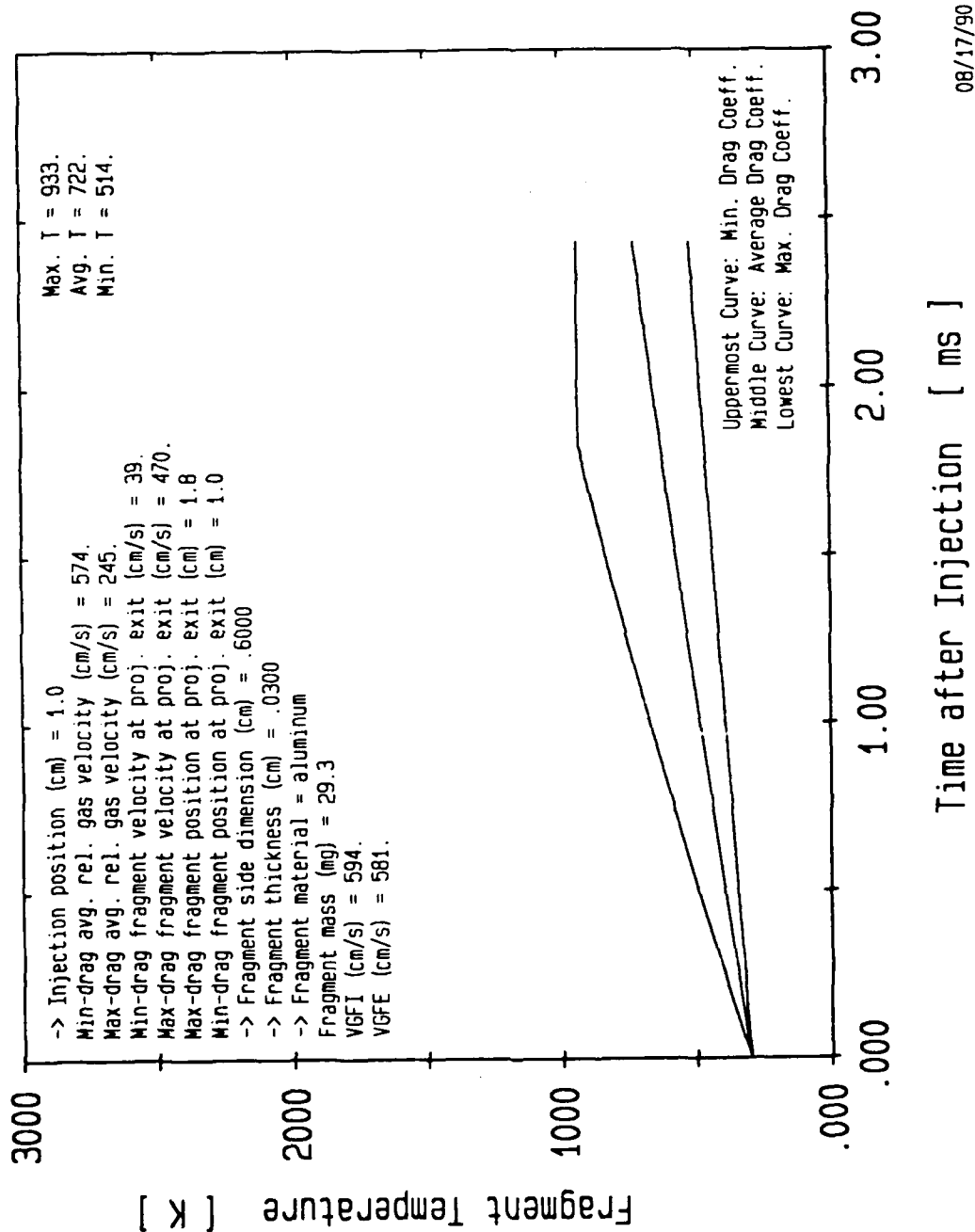
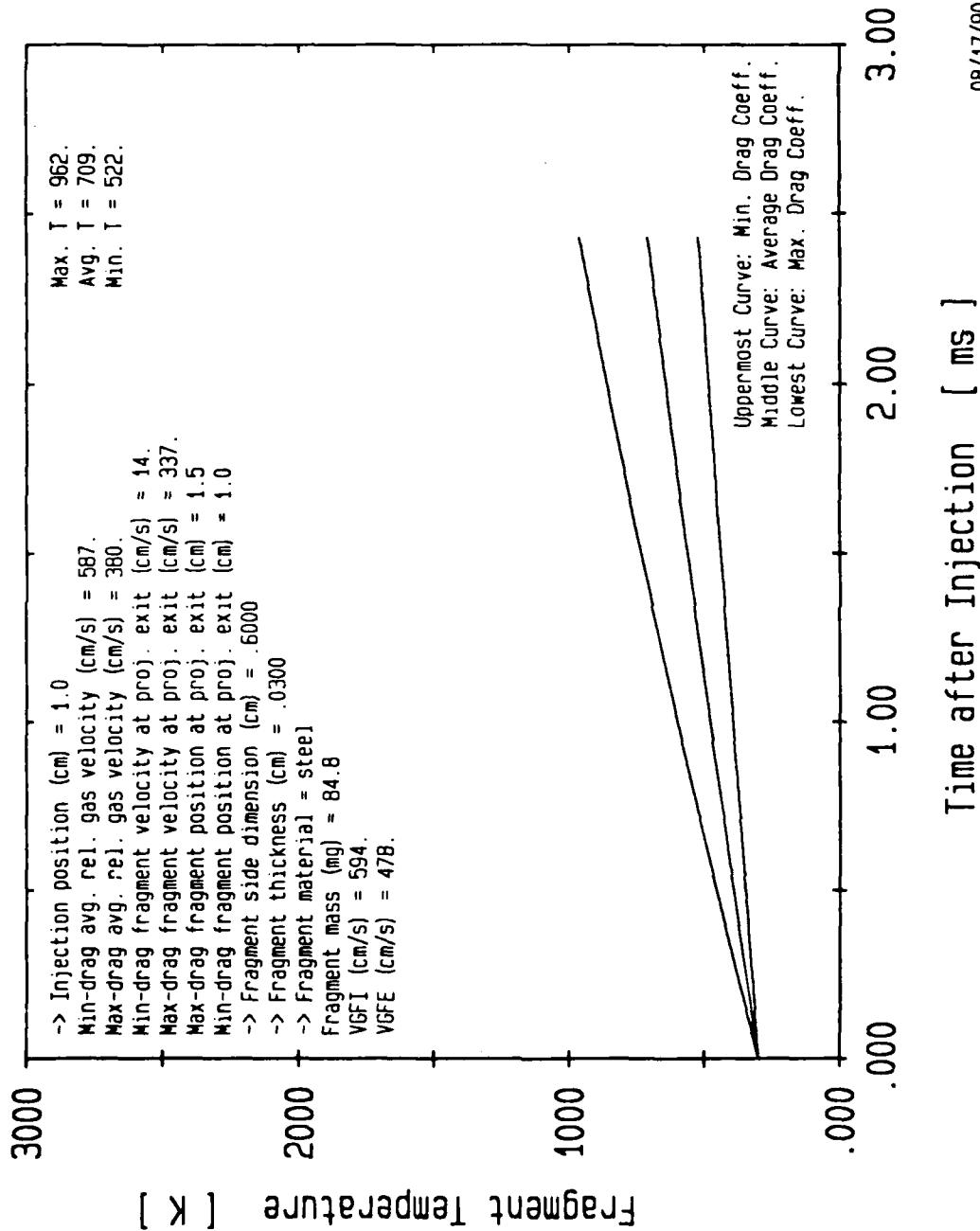


Fig. 15. Temperature history of aluminum fragment ($s = .6$ mm, $d = .03$ mm) originating near the breech

M829 : Fragment near Breech



08/17/90

Fig. 16. Temperature history of steel fragment ($s = .6$ cm, $d = .03$ cm) originating near the breech

M829 : Fragment at Case Mouth

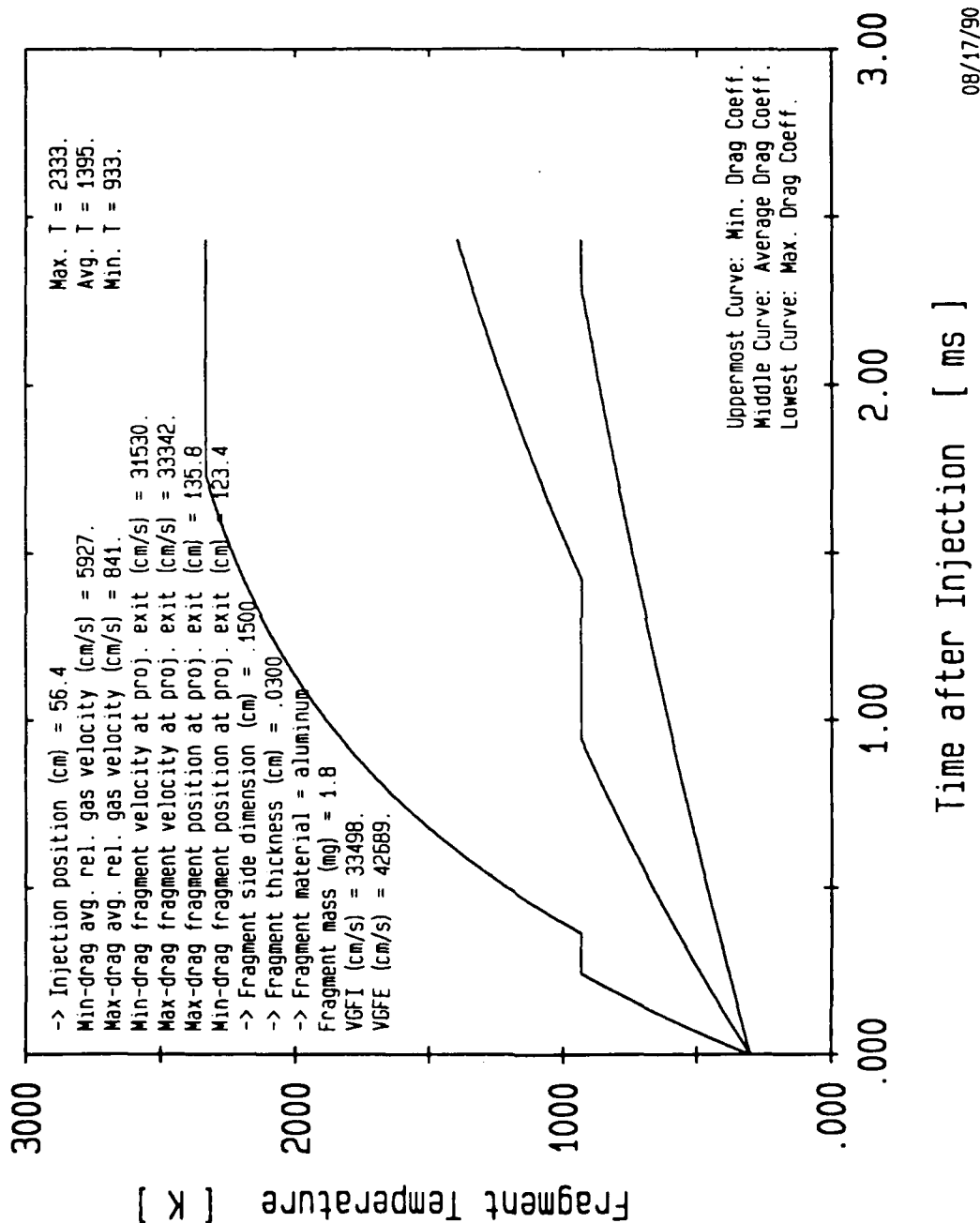
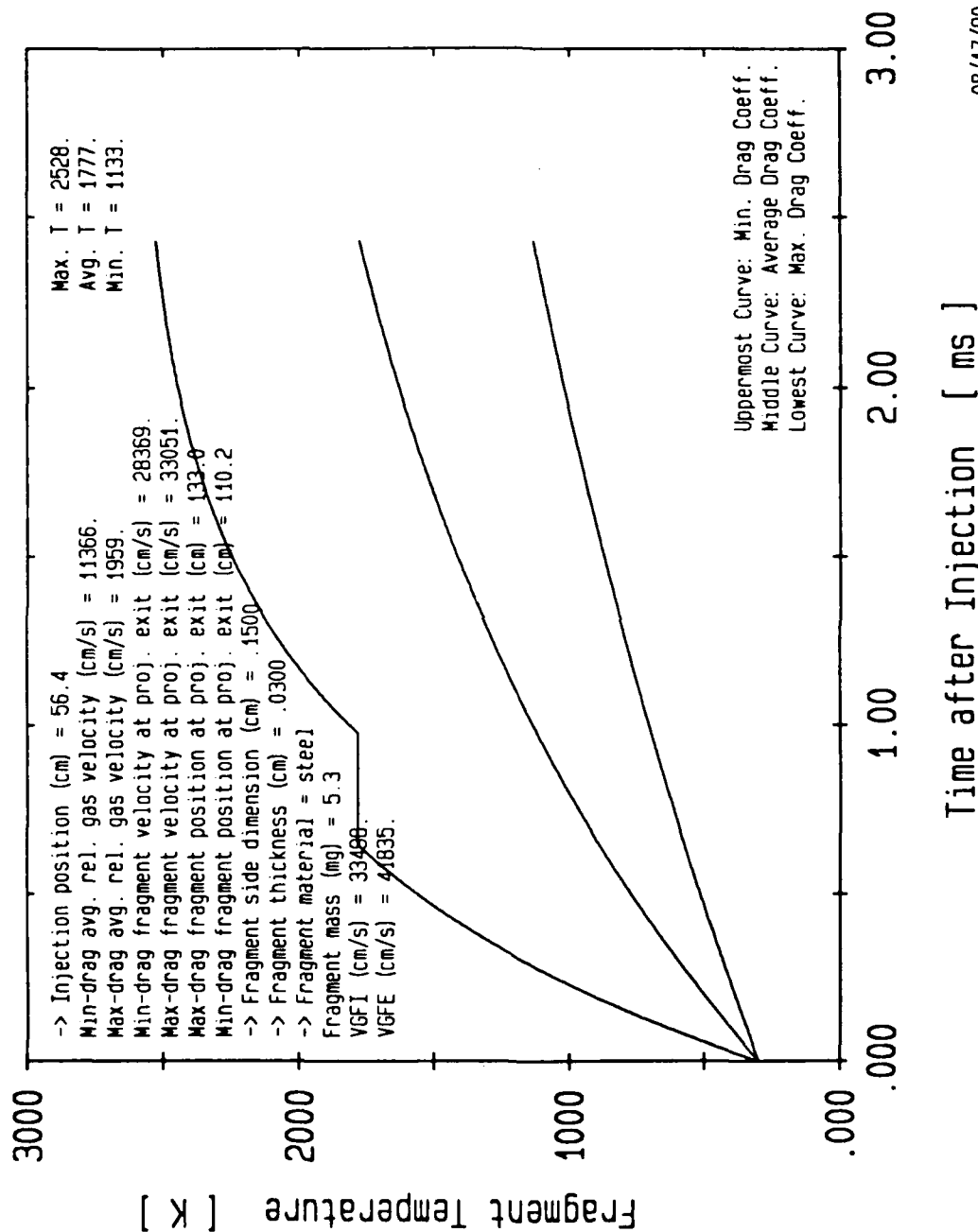


Fig. 17. Temperature history of aluminum fragment ($s = .15$ cm, $d = .03$ cm) originating at the case mouth

08/17/90

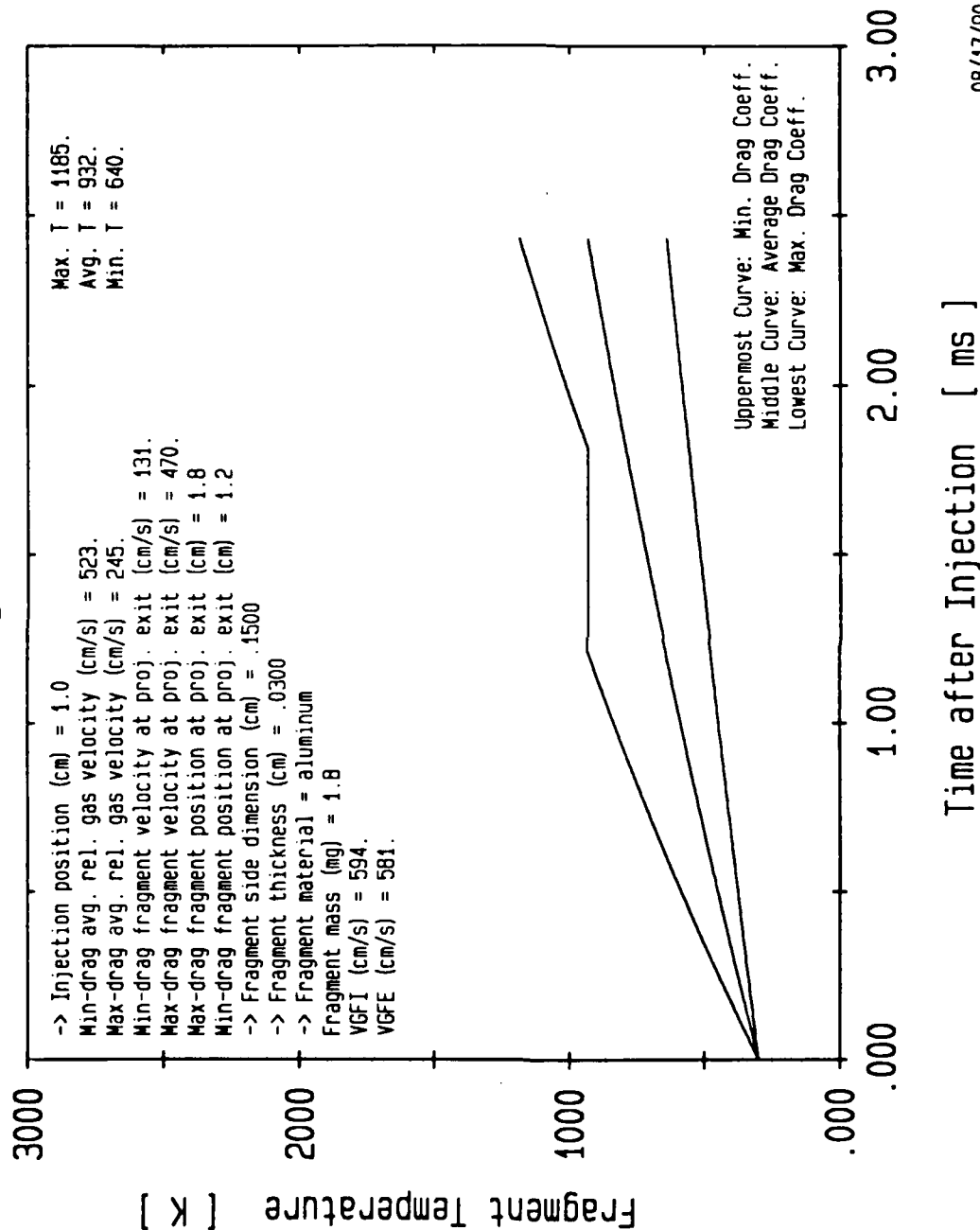
M829 : Fragment at Case Mouth



08/17/90

Fig. 18. Temperature history of steel fragment (s = .15 cm, d = .03 cm) originating at the case mouth

M829 : Fragment near Breech



08/17/90

Fig. 19. Temperature history of aluminum fragment ($s = .15$ cm, $d = .03$ cm) originating near the breech

M829 : Fragment near Breach

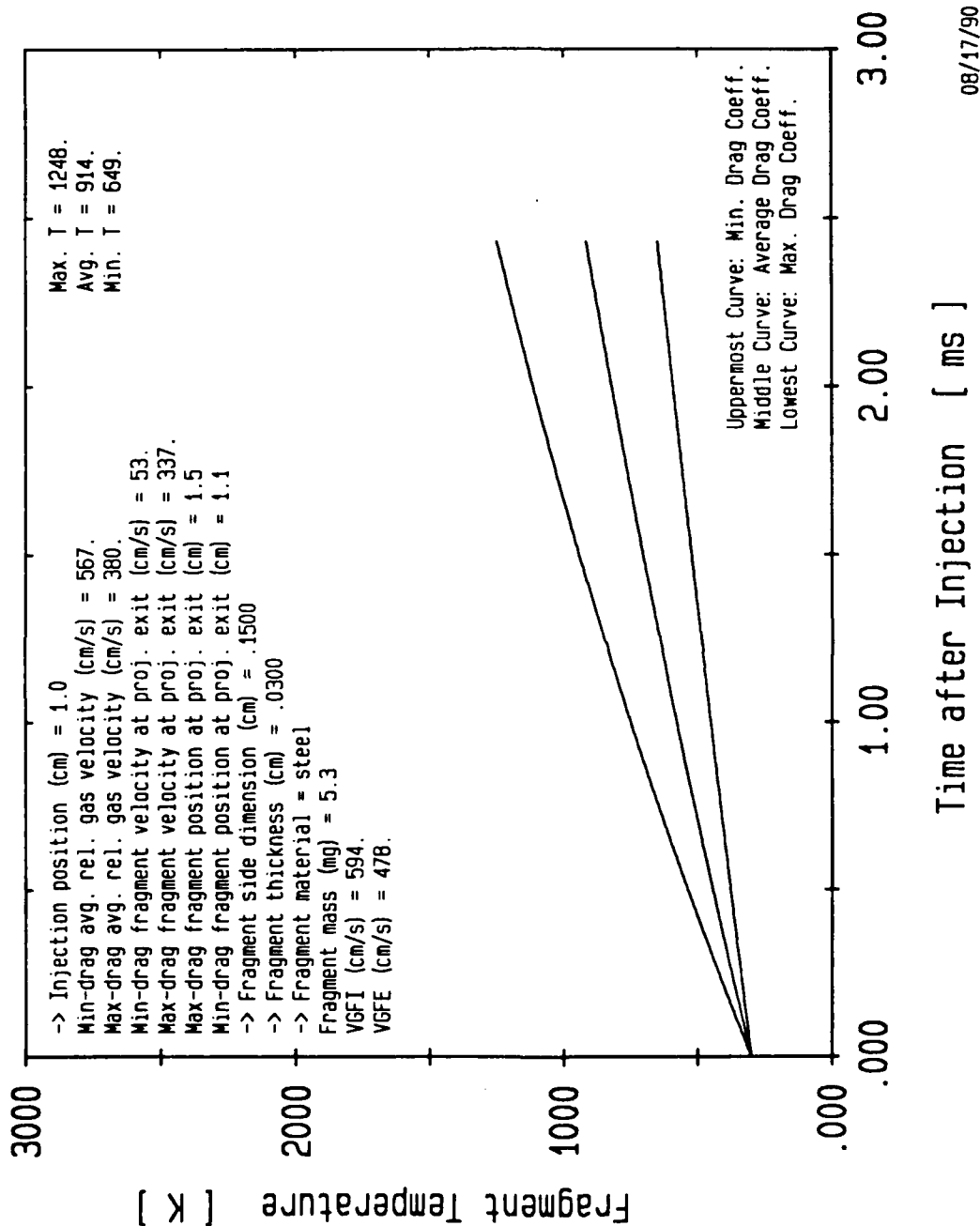


Fig. 20. Temperature history of steel fragment ($s = .15$ cm, $d = .03$ cm) originating near the breach

M829 : Fragment at Case Mouth

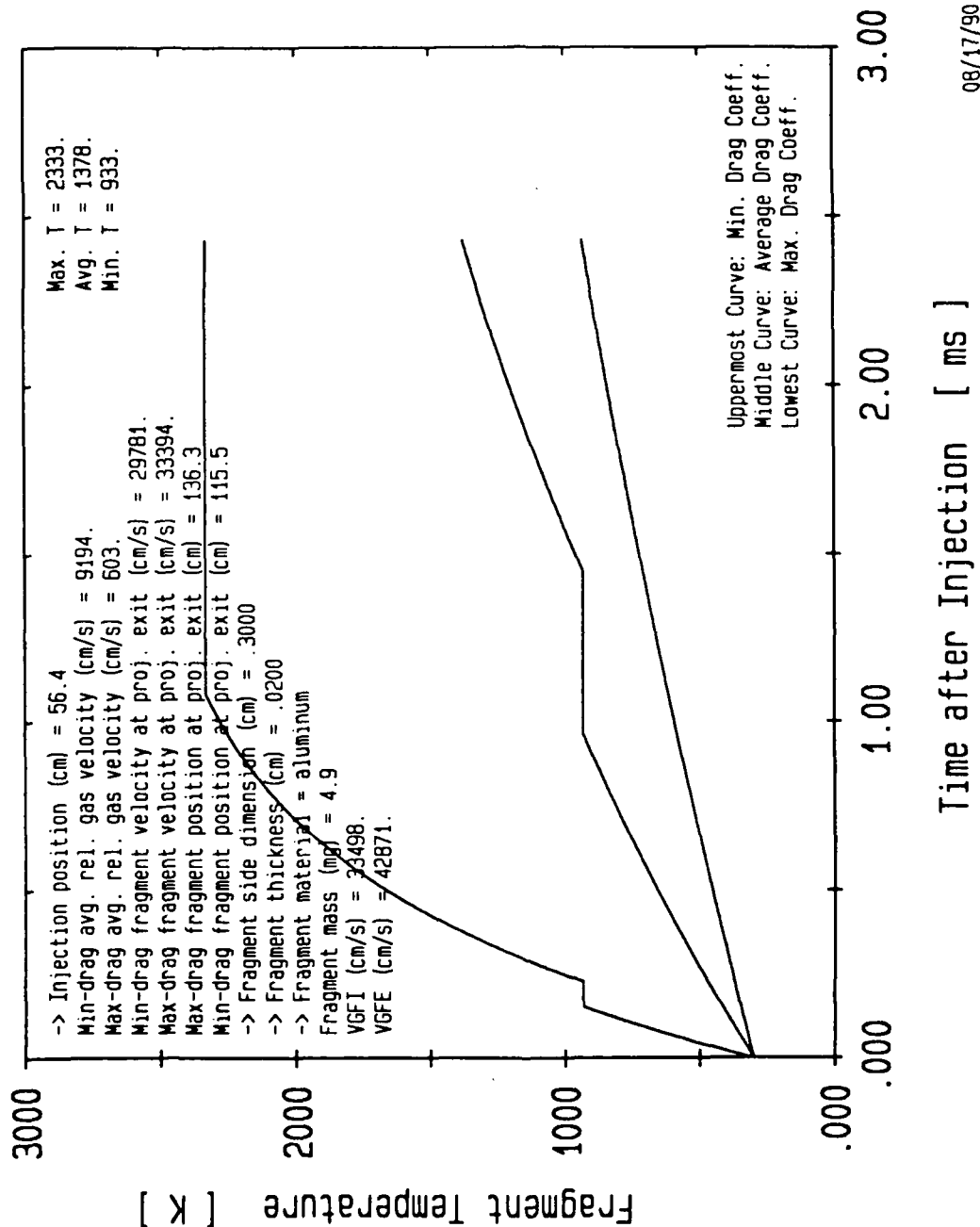


Fig. 21. Temperature history of aluminum fragment ($s = .3$ cm, $d = .02$ cm) originating at case mouth

M829 : Fragment at Case Mouth

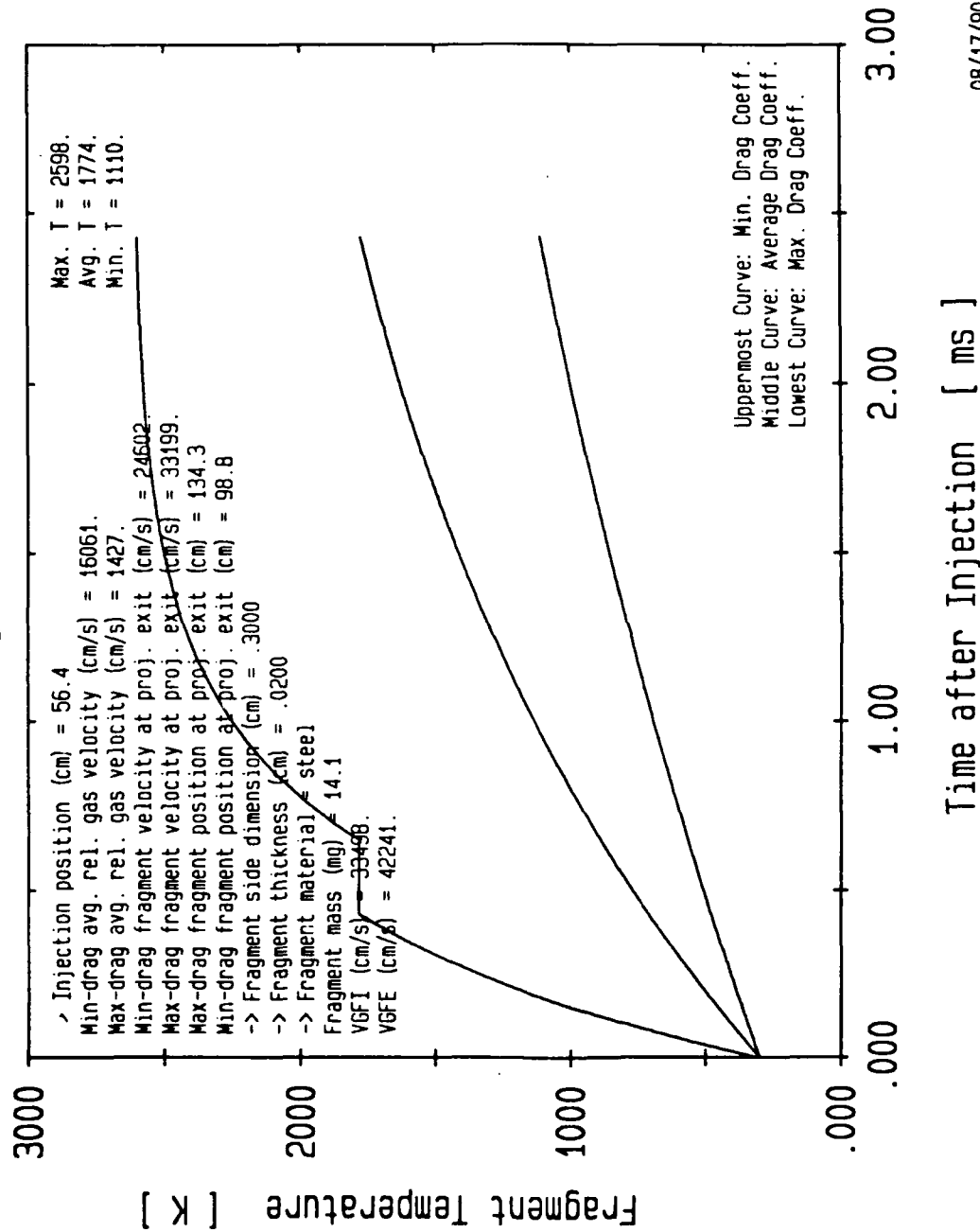
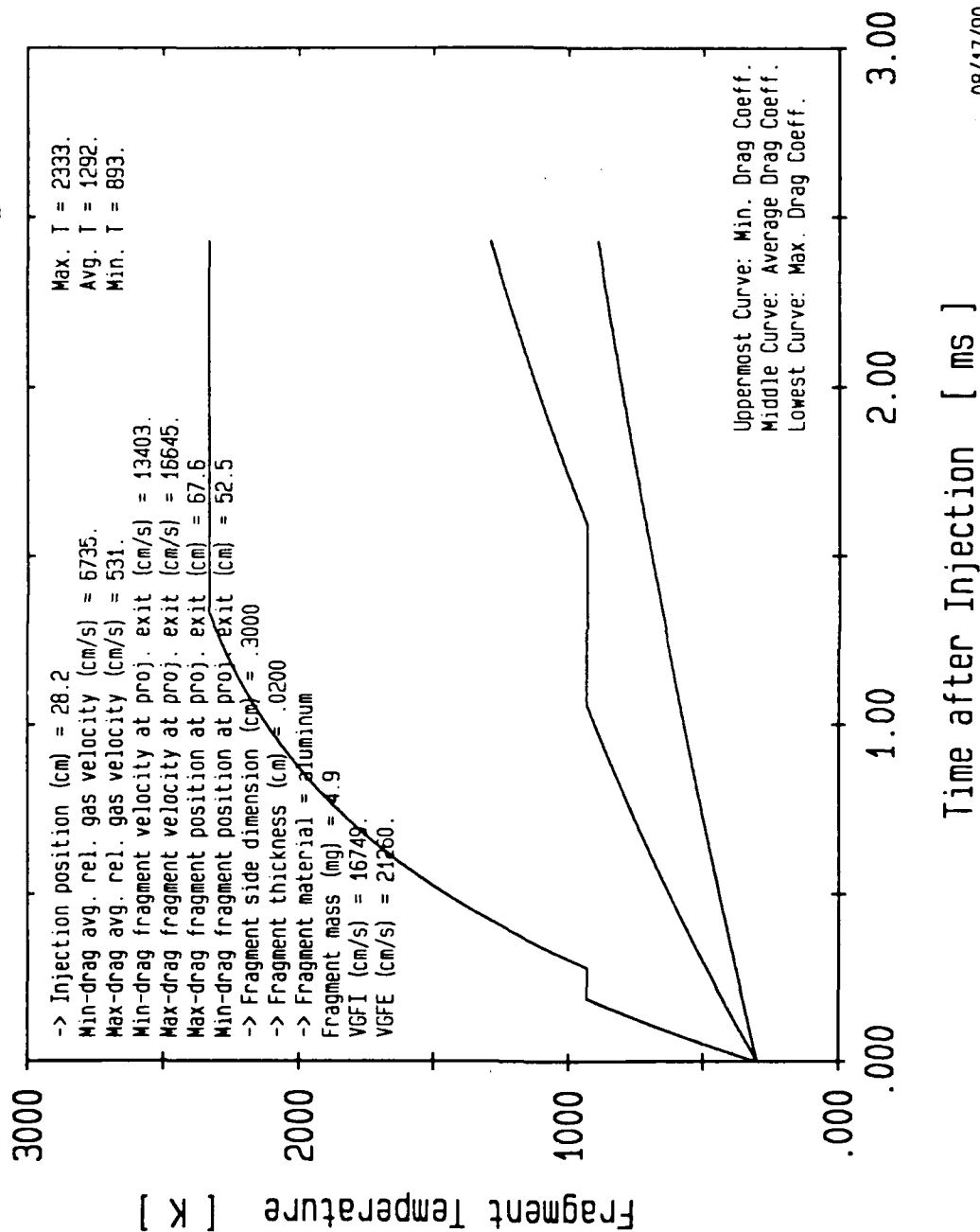


Fig. 22. Temperature history of steel fragment ($s = .3$ mm, $d = .02$ mm) originating at the case mouth

08/17/90

M829 : Fragment at Case Midlength



08/17/90

Fig. 23. Temperature history of aluminum fragment ($s = .3$ mm, $d = .02$ mm) originating at case midlength

M829 : Fragment at Case Midlength

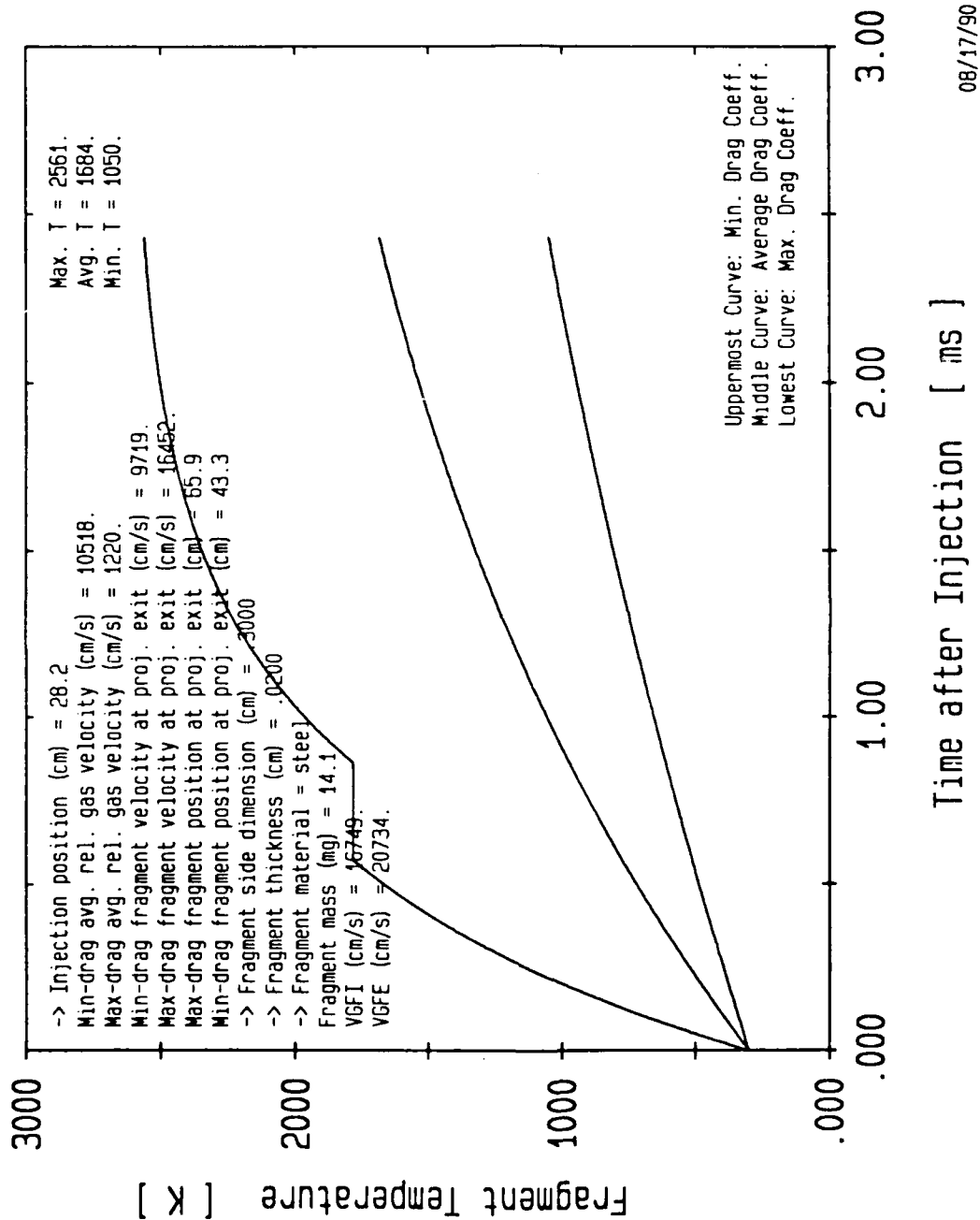


Fig. 24. Temperature history of steel fragment ($s = .3$ cm, $d = .02$ cm) originating at case midlength

M829 : Fragment near Breech

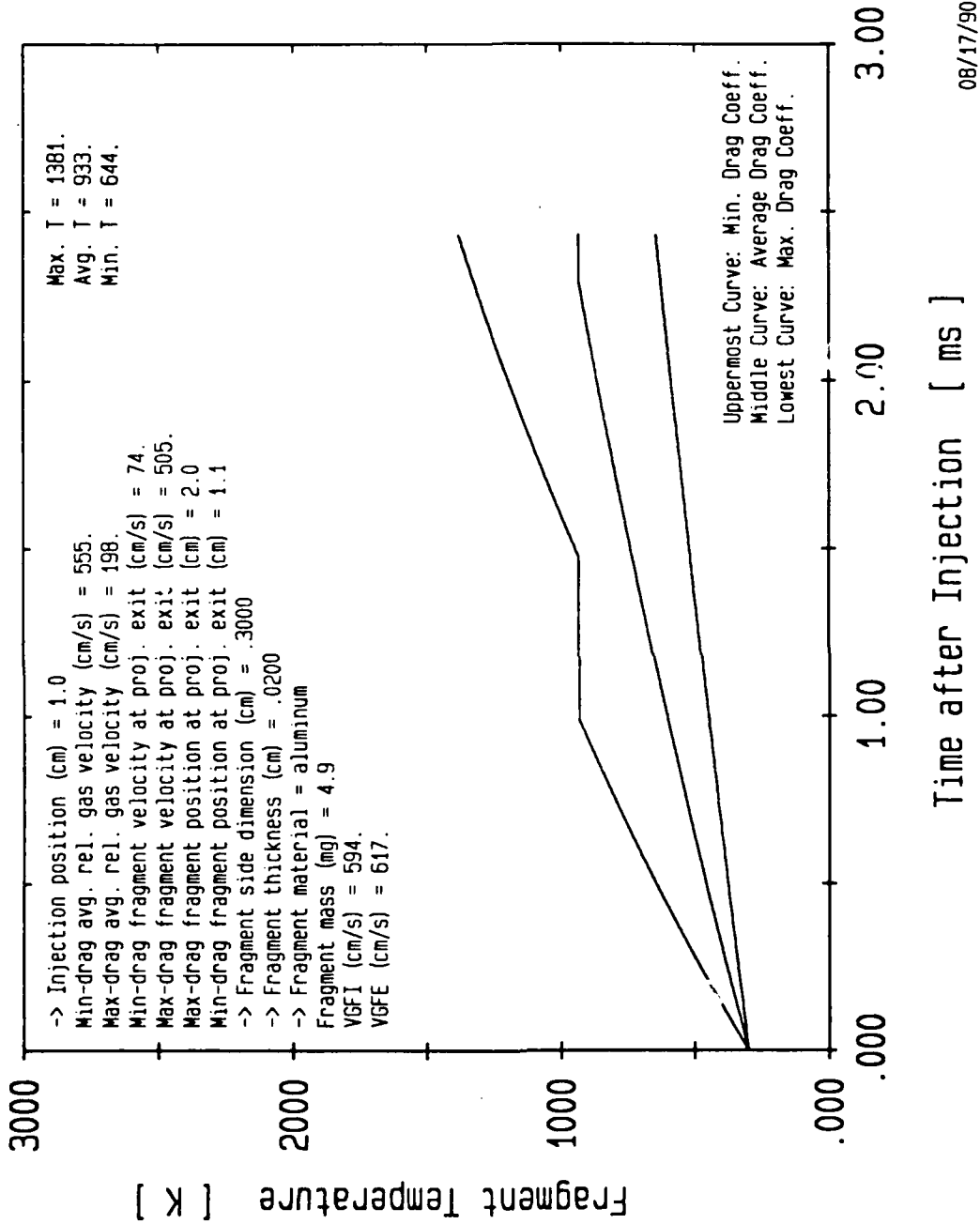
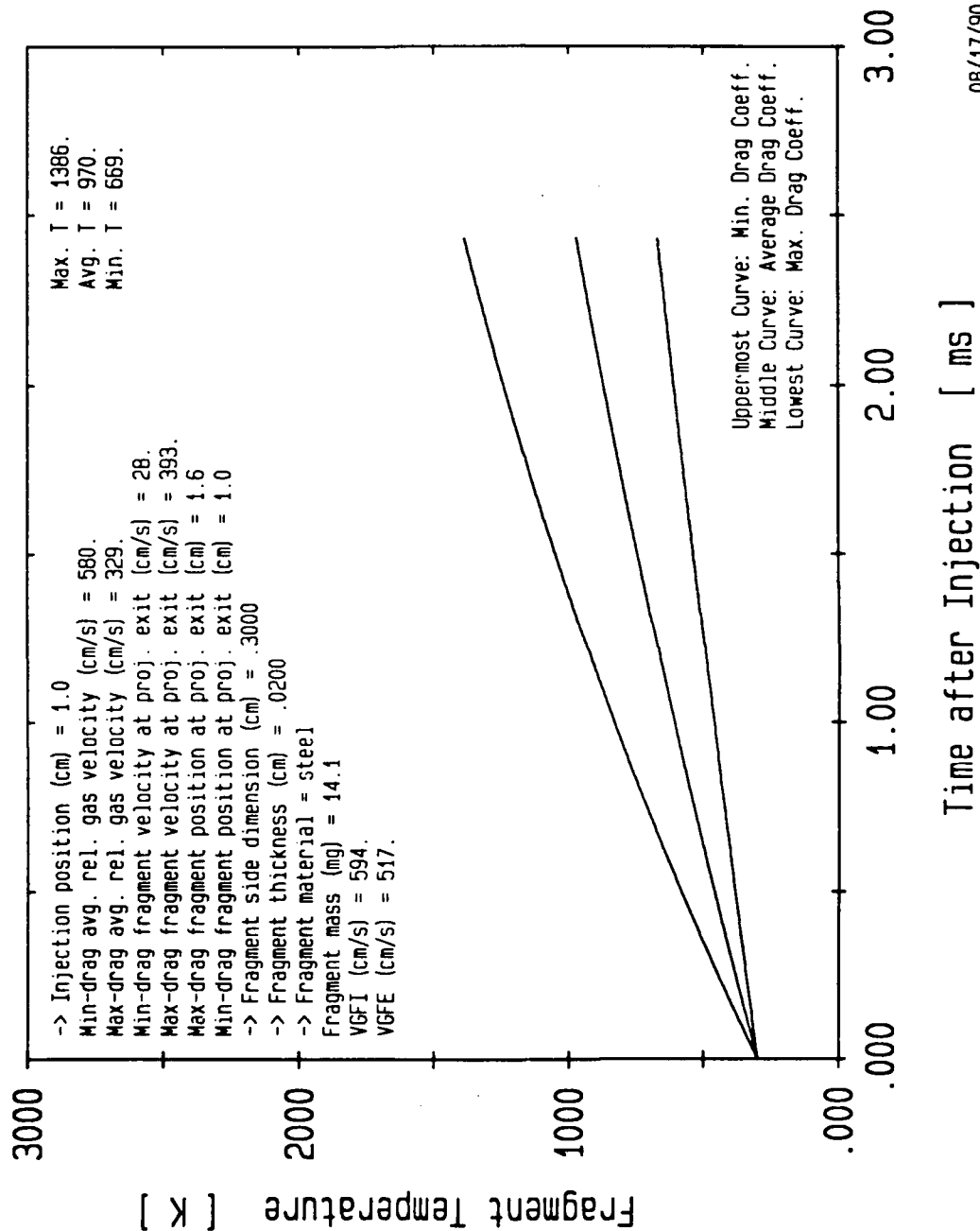


Fig. 25. Temperature history of aluminum fragment ($s = .3$ cm, $d = .02$ cm) originating near the breech

M829 : Fragment near Breech



08/17/90

Fig. 26. Temperature history of steel fragment ($s = .3$ cm, $d = .02$ cm) originating near the breech

M829 : Fragment at Case Mouth

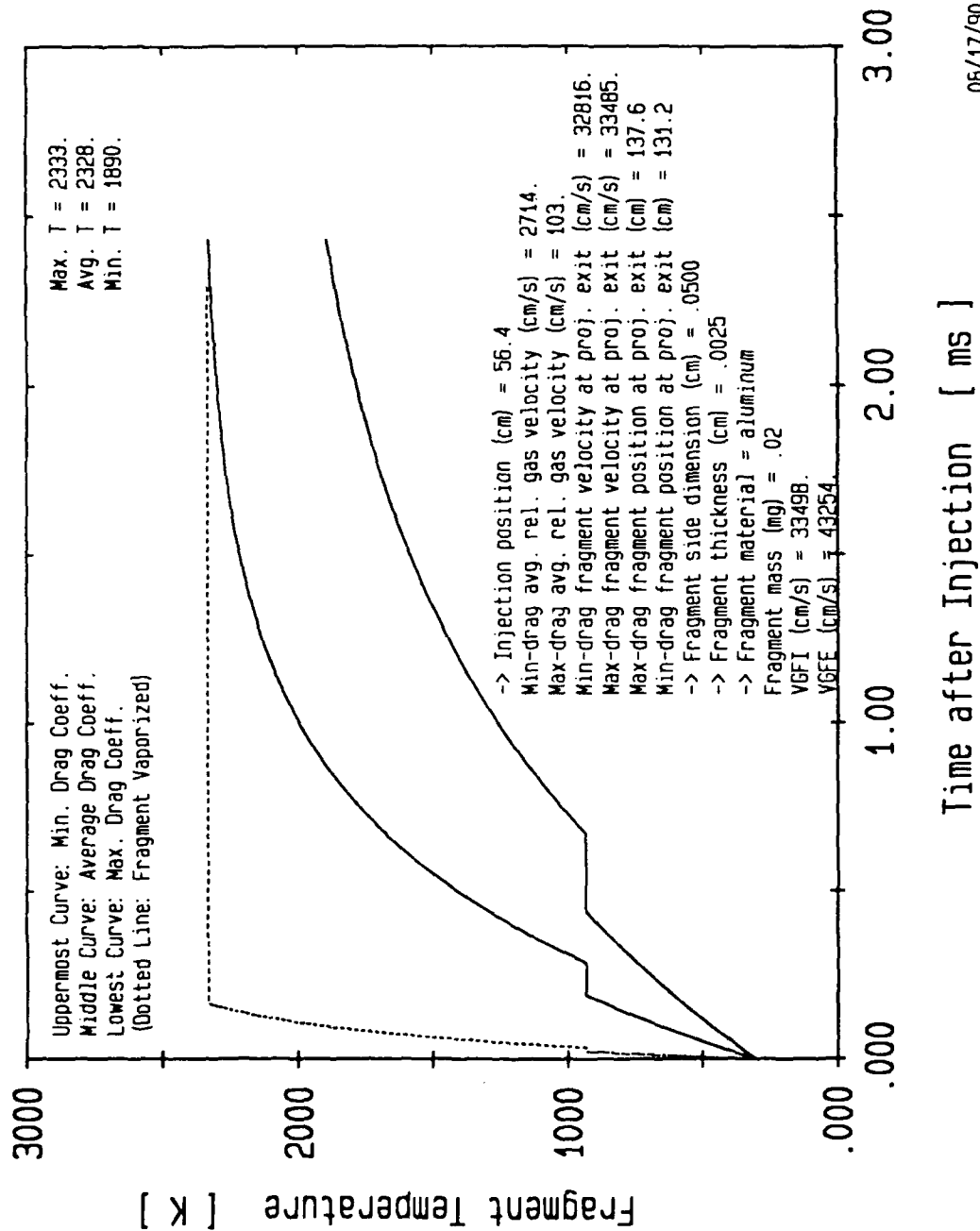


Fig. 27. Temperature history of aluminum fragment ($s = .05$ cm, $d = .0025$ cm) originating at the case mouth

M829 : Fragment at Case Mouth

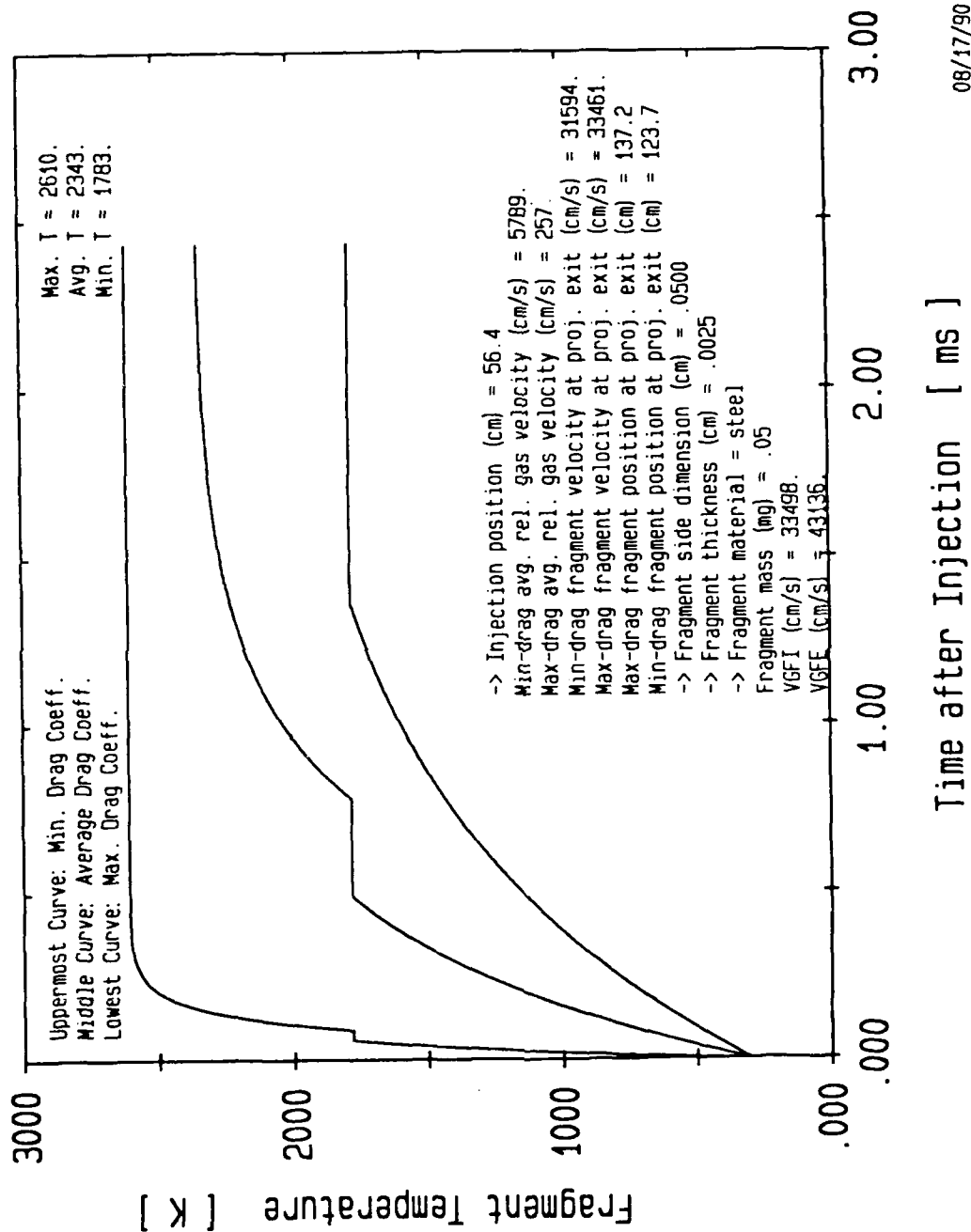
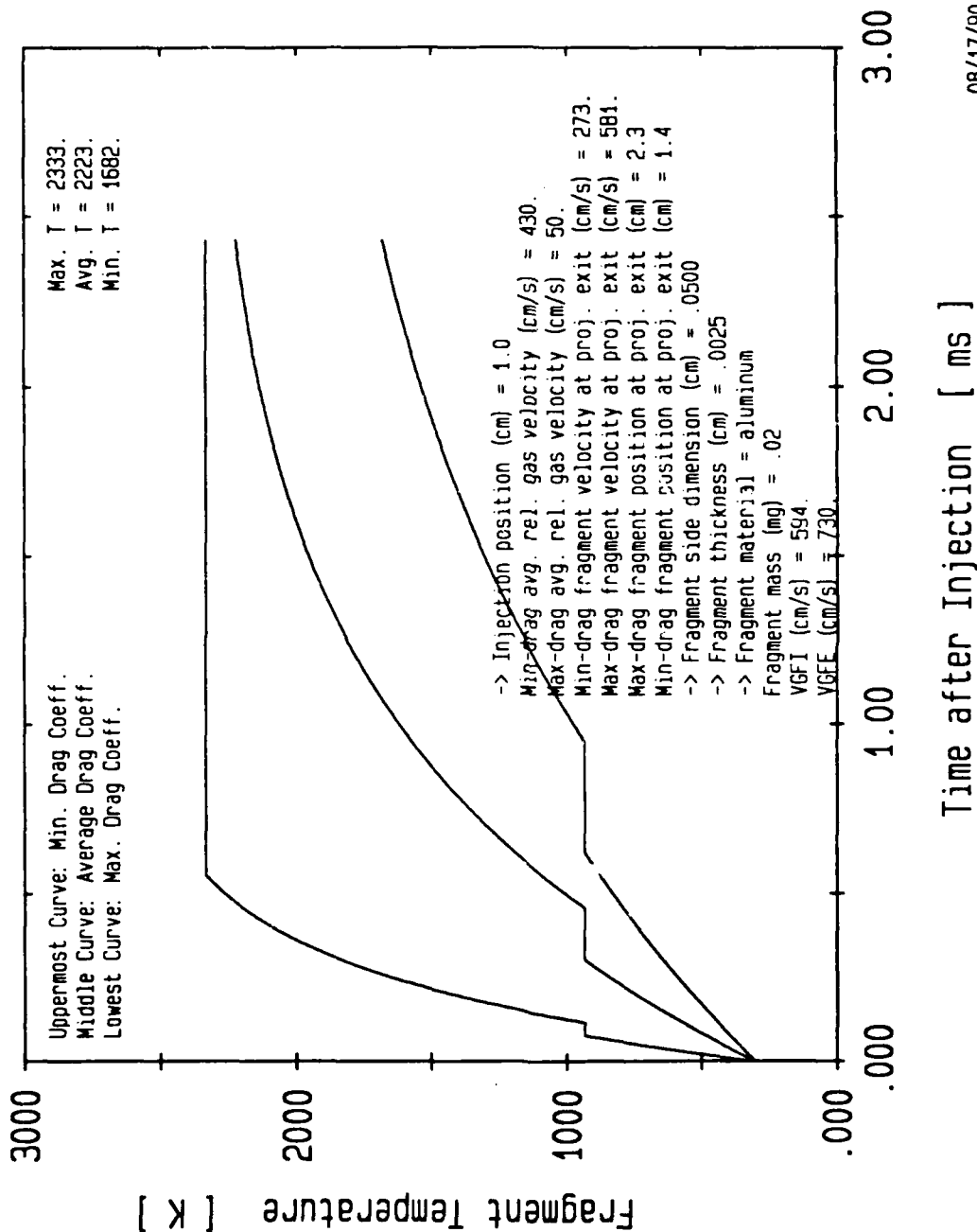


Fig. 28. Temperature history of steel fragment ($s = .05$ cm, $d = .0025$ cm) originating at the case mouth

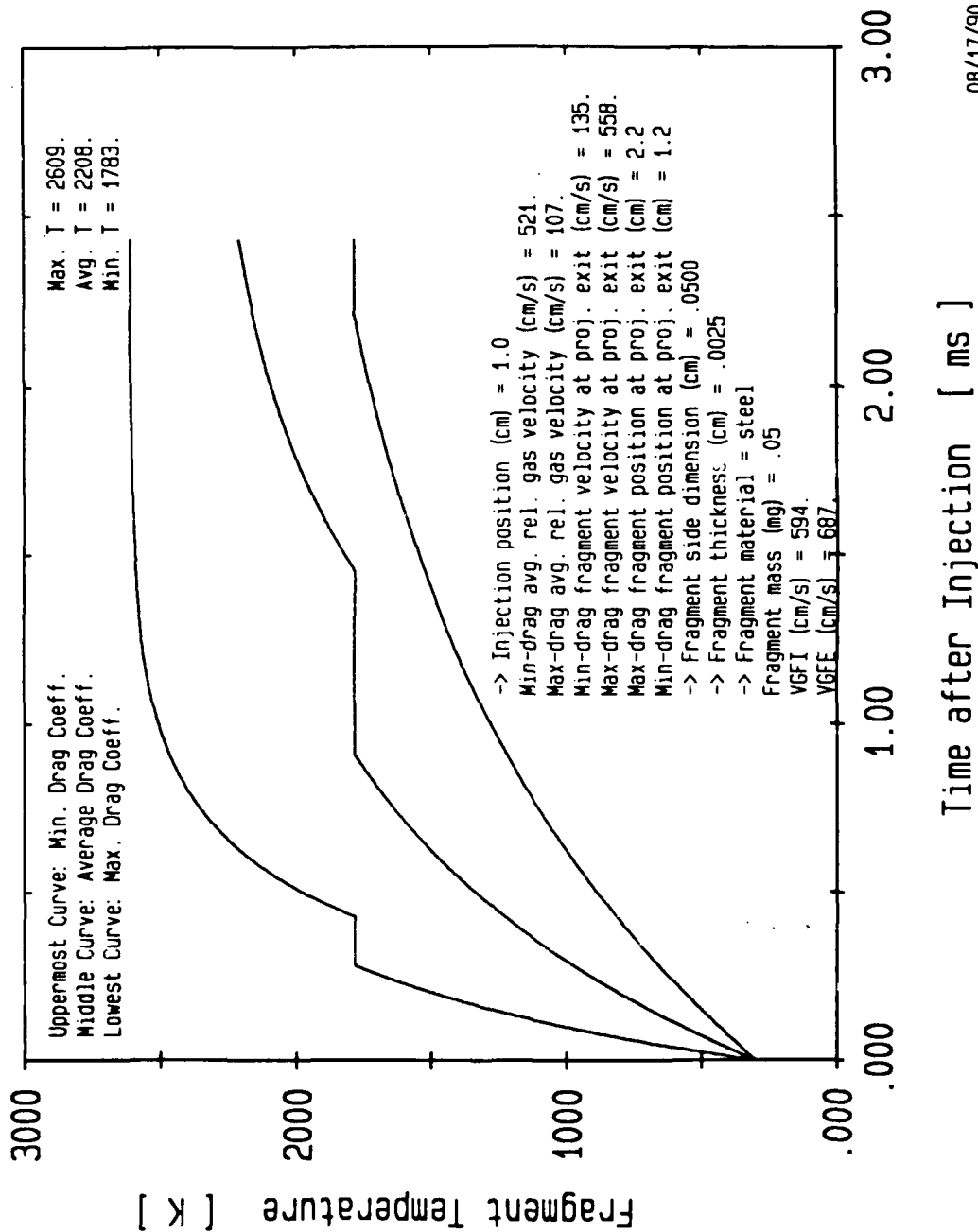
M829 : Fragment near Breech



08/17/90

Fig. 29. Temperature history of aluminum fragment ($s = .05$ cm, $d = .0025$ cm) originating at the breech

M829 : Fragment near Breech



08/17/90

Fig. 30. Temperature history of steel fragment (s = .05 cm, d = .0025 cm) originating at the breech

The calculations reported here are intended to examine the conditions under which the fragments are most likely to survive vaporization and, hence, the fragments are assumed to be imbedded at the outer radius of the case, though different axial locations are considered. Results of these calculations show that, for this outer-radius position, only very small fragments, near the limits of unaided visual inspection, will undergo complete vaporization. Particles imbedded near the case mouth will achieve the highest temperatures due to the high gas velocity there; however, these particles will also have the highest forward velocity at the time of projectile exit and therefore are most likely to be ejected from the barrel. Fragments imbedded near the breech are the ones most likely to be retained in the chamber after functioning of the propelling charge and these fragments will present a spectrum of ignition threats from smaller particles with relatively low internal energy at very high temperatures (>2000 K) to larger particles with relatively high internal energy but moderate temperatures (~ 500 K). Ignition probabilities for particles up to 1275 K in contact with combustible-case materials could be measured using the Hot Fragment Conductive Ignition Test^{4,5} (HFCIT) developed at BRL under the LOVA program. The test shows an inverse relationship between fragment mass and its temperature required to ignite a given energetic material. The smallest fragment used in the HFCIT is a 130 mg steel ball bearing. Unpublished records at BRL from approximately the 1981 - 1983 period show that this "fragment" ignited U.S. combustible-case material at a temperature of 850 K. A wafer shape likely would require a higher temperature due to its higher surface-to-volume ratio. New techniques would have to be developed to measure the ignition potential of fragments hotter than 1275 K.

REFERENCES

1. A. Melvin, "The Transient Behavior of Small Thermocouples in Static Gas Environments", *British J. Applied Physics*, Vol. 2, pp. 1339 - 1343, 1969.
2. Gelperin and Ainstein, "Heat Transfer in Fluidized Beds", in Fluidization, edited by J. F. Davidson and D. Harrison, Academic Press, 1971.
3. Ronald D. Anderson and Kurt D. Fickie, "IBHVG2 -- A User's Guide", BRL Technical Report BRL-TR-2829, July 1987. Calculations for the M829 performed by Frederick W. Robbins, BRL.
4. S. Wise, J. J. Rocchio, and H. J. Reeves, "The Ignitability of Composite Nitramine Propellants", 17th JANNAF Combustion Meeting, CPIA Publication 329, Vol. III, pp. 457 - 475, 1980.
5. H. C. Law and J. J. Rocchio, "The Hot Fragment Conductive Ignition Test: A Means of Evaluating Propellant Vulnerability to Spall", 18th JANNAF Combustion Meeting, CPIA Publication 347, Vol. II, pp. 321 - 334, 1981.
6. S. Gordon and B. J. McBride, "Computer Program for Calculation of Complex Chemical Equilibrium Compositions, Rocket Performance, Incident and Reflected Shocks, and Chapman-Jouguet Detonations", NASA Report SP-273, March 1976. Calculations performed by Stephen W. Bunte, BRL.
7. T. Baumeister and L. S. Marks, editors, Standard Handbook for Mechanical Engineers, McGraw-Hill, New York, 1967.
8. A. Goldsmith, T. E. Waterman, and H. J. Hirschhorn, Handbook of Thermophysical Properties of Solid Materials, Macmillan, New York, 1961.

INTENTIONALLY LEFT BLANK

APPENDIX 1: Interior Ballistic Calculations for the M829

INTENTIONALLY LEFT BLANK

APPENDIX 1: Interior Ballistic Calculations for the M829

Results of IBHVG2 calculations³ for the M829 round, performed at BRL, are shown in Figs. A1 - A6. This is a one-dimensional code that assumes spatially uniform but time-varying pressures and temperatures in the gun chamber.

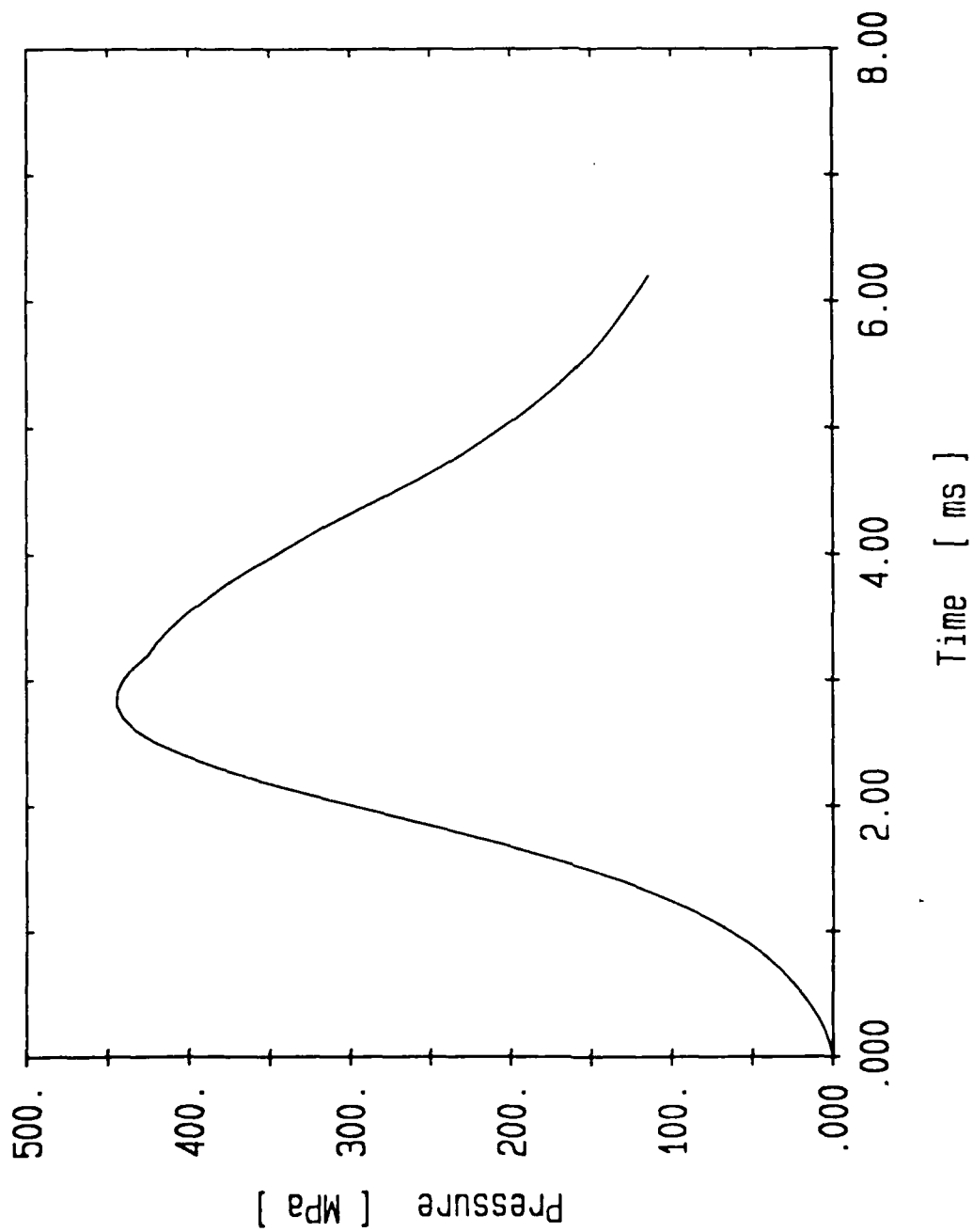


Fig. A-1. M829 Mean Pressure (IBHVG2)

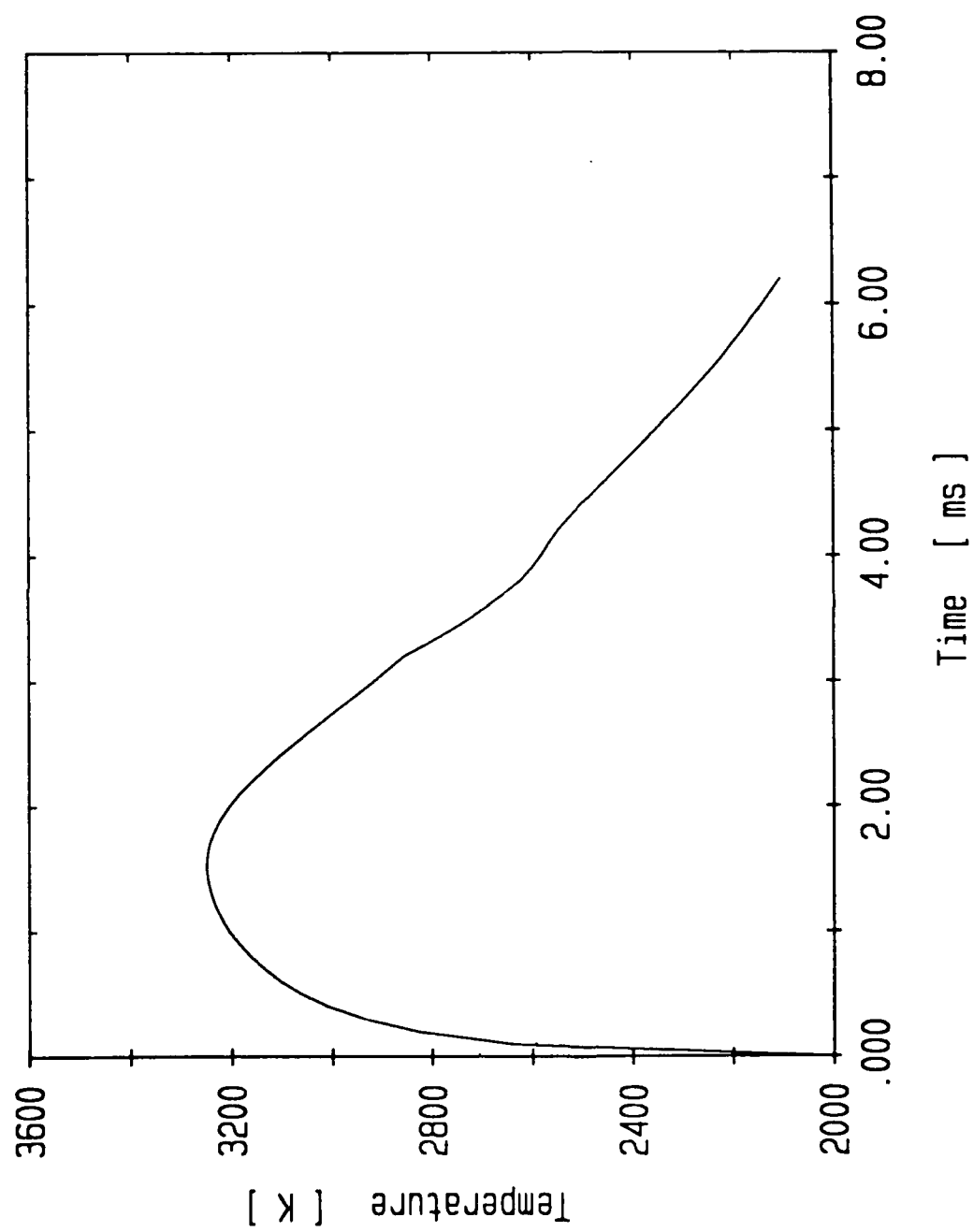


Fig. A-2. M829 Mean Temperature (IBHVG2)

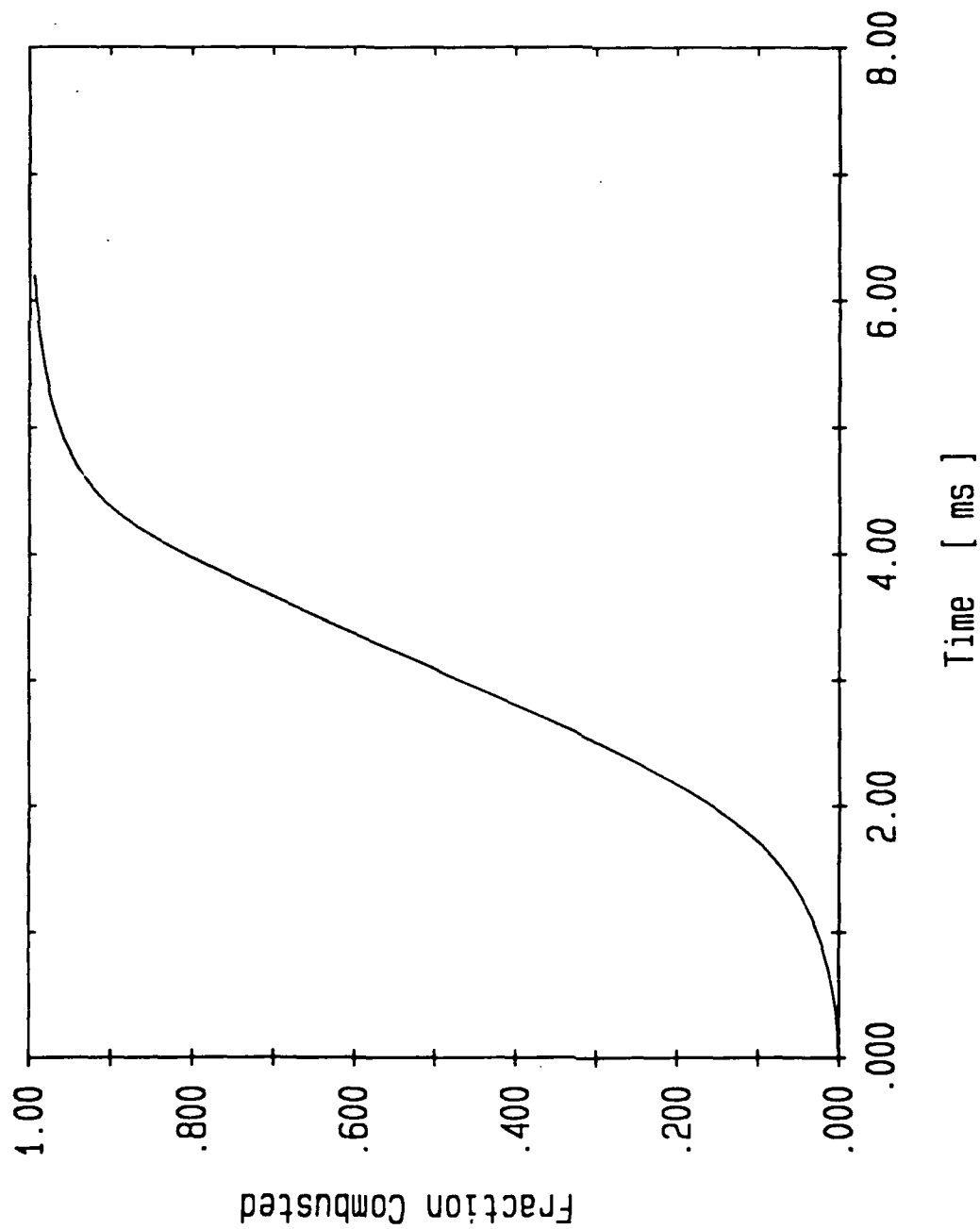


Fig. A-3. M829 Propellant Consumption (IBHVG2)

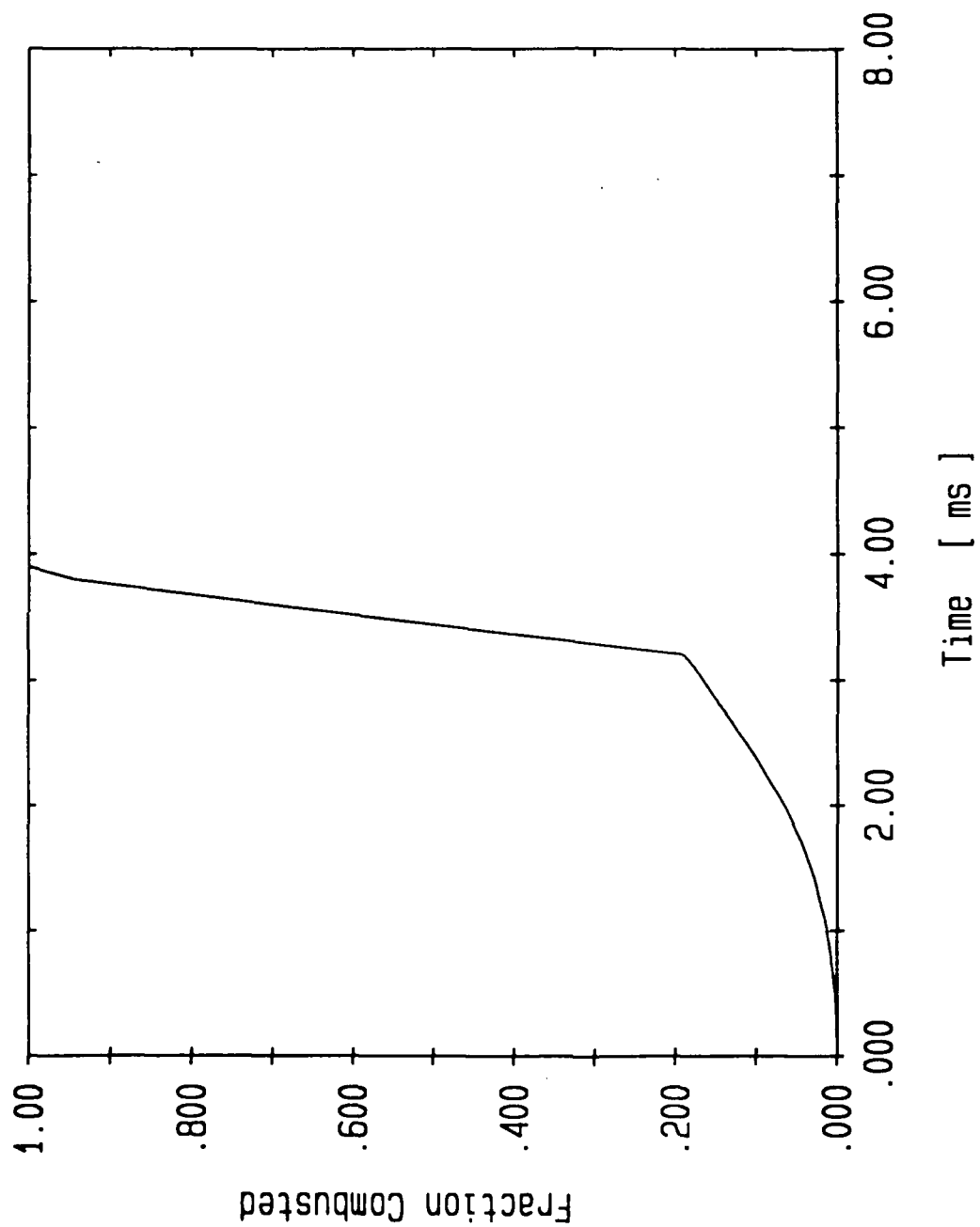


Fig. A-4. M829 Case Consumption (IBHVG2)

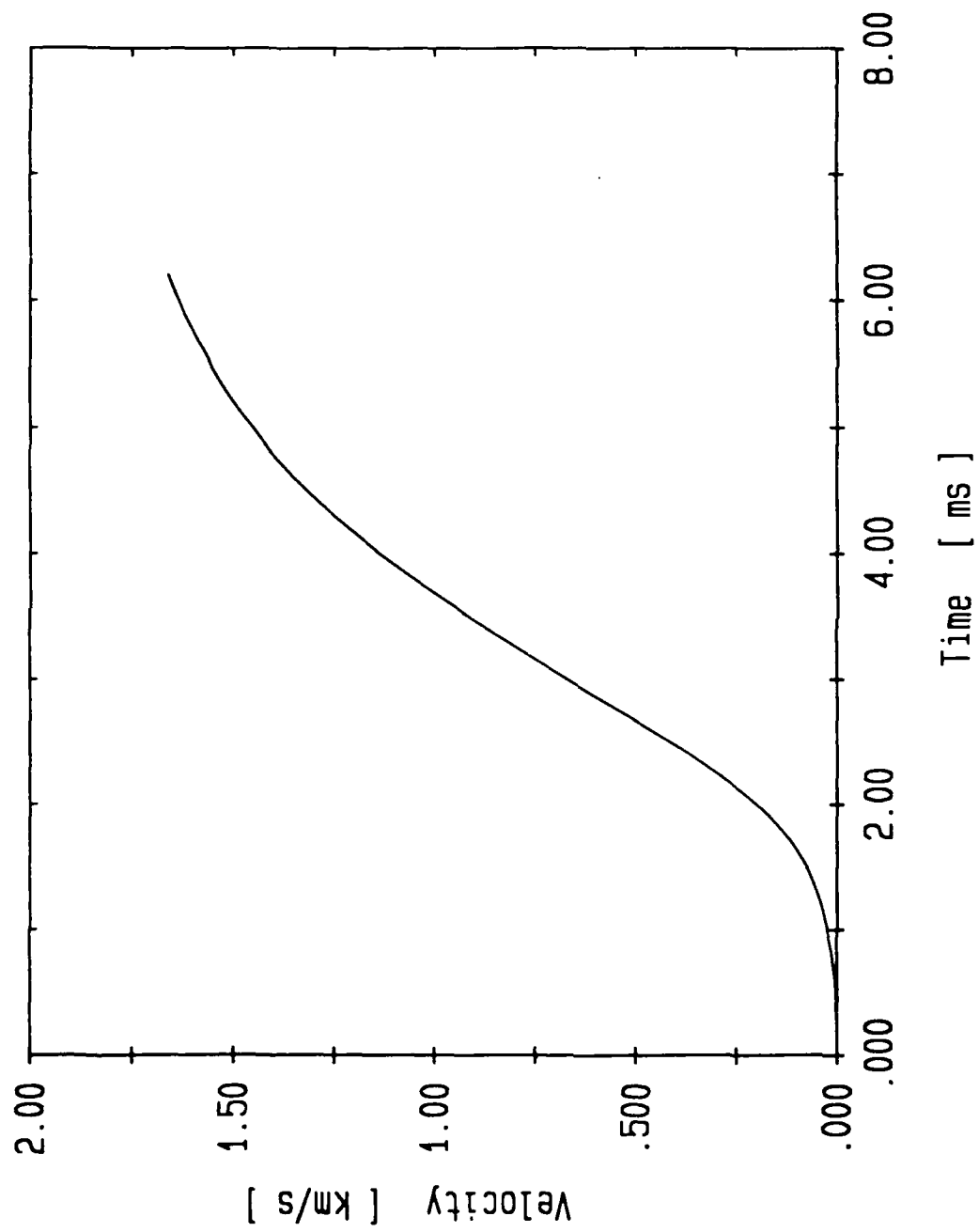


Fig. A-5. M829 Projectile Velocity (IBHVG2)

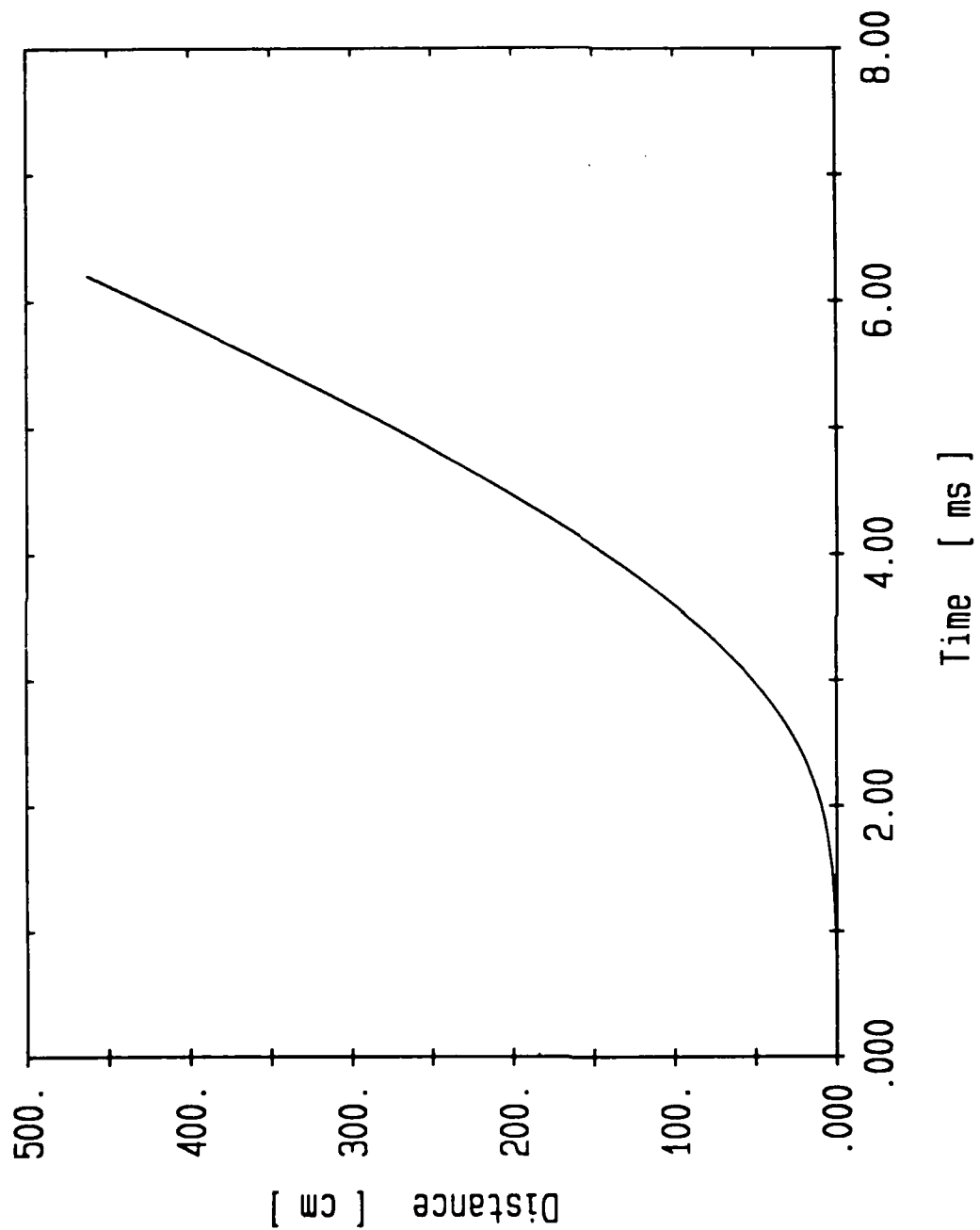


Fig. A-6. M829 Projectile Travel (IBHVG2)

INTENTIONALLY LEFT BLANK

APPENDIX 2: Numerical Parameter Values Used in Computations

INTENTIONALLY LEFT BLANK

APPENDIX 2: Numerical Parameter Values Used in Computations

Interior Ballistic Conditions³:

$P = 3670$ atm mean pressure at combustible-case burnout
 $T = 2610$ K mean temperature at combustible-case burnout
 $v_p = 3525$ ft/s = $1.07E5$ cm/s projectile velocity at case burnout
 $P = 1100$ atm mean pressure at projectile exit
 $T = 2090$ K mean temperature at projectile exit
 $v_p = 5481$ ft/s = $1.67E5$ cm/s projectile velocity at projectile exit
 $\tau_c = 2.43$ ms from time of case burnout to projectile exit

Gas Properties at Particular Conditions⁶:

$\lambda = .0056$ cal/cm-s-K for JA2 @ 2610 K & 3670 atm
 $\lambda = .0046$ cal/cm-s-K for JA2 @ 2090 K & 1100 atm
 $\mu = .0080$ g/s-cm for JA2 @ 2610 K & 3670 atm
 $\mu = .0068$ g/s-cm for JA2 @ 2090 K & 1100 atm
 $\rho_g = .427$ g/cc for JA2 @ 2610 K & 3670 atm
 $\rho_g = .160$ g/cc for JA2 @ 2090 K & 1100 atm

Average Gas Properties:

$\lambda = .0051$ cal/cm-s-K
 $\mu = .0074$ g/s-cm
 $\rho_g = 0.294$ g/cc

Fragment Properties:

Aluminum:

$\rho = 2.71$ g/cc Alloy 1100 [Ref. 7]
 $c(T) = 0.185 + 1.18E-4 T$ cal/g-K in range 300 - 950 K [Ref. 8]
 $c = 0.340$ cal/g-K avg. value between T_0 and T_b , extrapolating previous equation
 $T_m = 1220$ F = 660 C = 933 K melt. temp. [Ref. 7]
 $T_b = 3740$ F = 2060 C = 2333 K boiling pt. [Ref. 7]
 $\Delta H_{fusion} = 90$ cal/g heat of fusion [Ref. 8]
 $\Delta H_{vap} = 2720$ cal/g heat of vaporization [Ref. 8]
 $\epsilon = .05$ @ ~ 1000 K for cleaned surface [Ref. 8]

Steel:

$\rho = 7.85$ g/cc steel, AISI C1020 (hot worked) [Ref. 7]
 $c = 0.15$ cal/g-K avg. value between T_0 and T_f for plain carbon steel 0.2 - 0.6 % C [Ref. 8]
 $T_m = 2750$ F = 1510 C = 1783 K melt. temp. steel [Ref. 7]
 $T_m = 1400 - 1765$ K for plain carbon steel 2.0 - 0.1 % C [Ref. 8]
 $\Delta H_{fusion} = 65$ cal/g heat of fusion for iron [Ref. 8]

Constants:

$\sigma = 1.356E-12$ cal/cm²-s-K⁴ Stefan-Boltzmann const.

INTENTIONALLY LEFT BLANK

LIST OF SYMBOLS

a	radius of sphere of surface area A
c	fragment heat capacity (cal/g-K)
d	fragment thickness (cm)
h	heat transfer coefficient (cal/cm ² -K-s)
s	fragment side dimension (assuming square shape)
t	time, referenced to beginning of interior-ballistic cycle
t_e	time of projectile exit from barrel
t_i	time of fragment injection into interior-ballistic flow
v_f	fragment velocity
v_g	velocity of combustion gases
v_{gf}	velocity of combustion gases at the fragment position
v_p	velocity of projectile
x	position in chamber/tube relative to breech block
x_f	location of fragment
x_g	location of gas particle (combustion fluid) which passes x_i at t_i
x_i	location of fragment at injection
A	fragment surface area
A_s	fragment sectional area
ΔH_{fusion}	fragment heat of fusion (cal/g)
ΔH_{vap}	fragment heat of vaporization (cal/g)
L_c	length of chamber
Nu	Nusselt number
Pr	Prandtl number
Re	Reynolds number
T	temperature of fragment (K)
T_b	fragment boiling point (K)
T_g	temperature of the gas at some specified position in the chamber/bore
T_{gf}	temperature of the gas in contact with the fragment
T_m	fragment melting point (K)
T_0	initial temperature of fragment
V	= $Ad/2$, fragment volume
ϵ	fragment emissivity
Θ	= $T_{gf} - T$
λ	thermal conductivity of the combustion gases
μ	viscosity of combustion gases
ξ_p	distance traveled by projectile
ρ	fragment density (g/cc)
ρ_g	density of combustion gases
σ	Stefan-Boltzmann constant
τ	time, reference to instant of fragment injection into flow
τ_e	time of projectile exit
$\langle \rangle$	average of enclosed variable

INTENTIONALLY LEFT BLANK

No of Copies	Organization
2	Administrator Defense Technical Info Center ATTN: DTIC-DDA Cameron Station Alexandria, VA 22304-6145
1	HQDA (SARD-TR) WASH DC 20310-0001
1	Commander US Army Materiel Command ATTN: AMCDRA-ST 5001 Eisenhower Avenue Alexandria, VA 22333-0001
1	Commander US Army Laboratory Command ATTN: AMSLC-DL Adelphi, MD 20783-1145
2	Commander US Army, ARDEC ATTN: SMCAR-IMI-I Picatinny Arsenal, NJ 07806-5000
2	Commander US Army, ARDEC ATTN: SMCAR-TDC Picatinny Arsenal, NJ 07806-5000
1	Director Benet Weapons Laboratory US Army, ARDEC ATTN: SMCAR-CCB-TL Watervliet, NY 12189-4050
1	Commander US Army Armament, Munitions and Chemical Command ATTN: SMCAR-ESP-L Rock Island, IL 61299-5000
1	Commander US Army Aviation Systems Command ATTN: AMSAV-DACL 4300 Goodfellow Blvd. St. Louis, MO 63120-1798

No of Copies	Organization
1	Director US Army Aviation Research and Technology Activity ATTN: SAVRT-R (Library) M/S 219-3 Ames Research Center Moffett Field, CA 94035-1000
1	Commander US Army Missile Command ATTN: AMSMI-RD-CS-R (DOC) Redstone Arsenal, AL 35898-5010
1	Commander US Army Tank-Automotive Command ATTN: AMSTA-TSL (Technical Library) Warren, MI 48397-5000
1	Director US Army TRADOC Analysis Command ATTN: ATRC-WSR White Sands Missile Range, NM 88002-5502
(Class. only)1	Commandant US Army Infantry School ATTN: ATSH-CD (Security Mgr.) Fort Benning, GA 31905-5660
(Unclass. only)1	Commandant US Army Infantry School ATTN: ATSH-CD-CSO-OR Fort Benning, GA 31905-5660
1	Air Force Armament Laboratory ATTN: AFATL/DLODL Eglin AFB, FL 32542-5000
	<u>Aberdeen Proving Ground</u>
2	Dir, USAMSAA ATTN: AMXSY-D AMXSY-MP, H. Cohen
1	Cdr, USATECOM ATTN: AMSTE-TD
3	Cdr, CRDEC, AMCCOM ATTN: SMCCR-RSP-A SMCCR-MU SMCCR-MSI
1	Dir, VLAMO ATTN: AMSLC-VL-D

No. of Copies	Organization
4	Commander US Army Research Office ATTN: R. Ghirardelli D. Mann R. Singleton R. Shaw P.O. Box 12211 Research Triangle Park, NC 27709-2211
2	Commander US Army, ARDEC ATTN: SMCAR-AEE-B, D.S. Downs SMCAR-AEE, J.A. Lannon Picatinny Arsenal, NJ 07806-5000
1	Commander US Army, ARDEC ATTN: SMCAR-AEE-BR, L. Harris Picatinny Arsenal, NJ 07806-5000
2	Commander US Army, ARDEC ATTN: SMCAR-CCH, J. DeLorenzo SMCAR-CCH-T, P. Christian Picatinny Arsenal, NJ 07806-5000
3	Commander US Army, ARDEC ATTN: SMCAR-CCH-V, B. Konrad Picatinny Arsenal, NJ 07806-5000
1	Commander US Army, ARDEC Benet Weapons Laboratory ATTN: SMCAR-CCB-DS, C.A. Andrade Watervliet, NY 12189-4050
1	Commander USA AMCCOM ATTN: AMSMC-QAT-A, C. Knutsen Picatinny Arsenal, NJ 07806-5000
1	Commander USA AMCCOM ATTN: AMSMC-ASR, R. Crawford Rock Island, IL 61249-6000
1	PEO-Armaments Project Manager Tank Main Armament Systems ATTN: SFAE-AR-TMA, K. Russell Picatinny Arsenal, NJ 07806-5000

No. of Copies	Organization
2	Commander US Army Missile Command ATTN: AMSMI-RK, DJ. Ifshin W. Wharton Redstone Arsenal, AL 35898
1	Commander US Army Missile Command ATTN: AMSMI-RKA, A.R. Maykut Redstone Arsenal, AL 35898-5249
1	Office of Naval Research Department of the Navy ATTN: R.S. Miller, Code 432 800 N. Quincy Street Arlington, VA 22217
1	Commander Naval Air Systems Command ATTN: J. Ramnarace, AIR-54111C Washington, DC 20360
1	Commander Naval Surface Warfare Center ATTN: J.L. East, Jr., G-23 Dahlgren, VA 22448-5000
2	Commander Naval Surface Warfare Center ATTN: R. Bernecker, R-13 G.B. Wilmot, R-16 Silver Spring, MD 20903-5000
5	Commander Naval Research Laboratory ATTN: M.C. Lin J. McDonald E. Oran J. Shnur R.J. Doyle, Code 6110 Washington, DC 20375
1	Commanding Officer Naval Underwater Systems Center Weapons Dept. ATTN: R.S. Lazar/Code 36301 Newport, RI 02840
2	Commander Naval Weapons Center ATTN: T. Boggs, Code 388 T. Parr, Code 3895 China Lake, CA 93555-6001

<u>No. of Copies</u>	<u>Organization</u>
1	Superintendent Naval Postgraduate School Dept. of Aeronautics ATTN: D.W. Netzer Monterey, CA 93940
3	AL/LSCF ATTN: R. Corley R. Geisler J. Levine Edwards AFB, CA 93523-5000
1	AL/MKPB ATTN: B. Goshgarian Edwards AFB, CA 93523-5000
1	AFOSR ATTN: J.M. Tishkoff Bolling Air Force Base Washington, DC 20332
1	OSD/SDIO/IST ATTN: L. Caveny Pentagon Washington, DC 20301-7100
1	Commandant USAFAS ATTN: ATSF-TSM-CN Fort Sill, OK 73503-5600
1	F.J. Seiler ATTN: S.A. Shackelford USAF Academy, CO 80840-6528
1	University of Dayton Research Institute ATTN: D. Campbell AL/PAP Edwards AFB, CA 93523
1	NASA Langley Research Center Langley Station ATTN: G.B. Northam/MS 168 Hampton, VA 23365
4	National Bureau of Standards ATTN: J. Hastie M. Jacob T. Kashiwagi H. Semerjian US Department of Commerce Washington, DC 20234
1	Aerojet Solid Propulsion Co. ATTN: P. Micheli Sacramento, CA 95813

<u>No. of Copies</u>	<u>Organization</u>
1	Applied Combustion Technology, Inc. ATTN: A.M. Varney P.O. Box 607885 Orlando, FL 32860
2	Applied Mechanics Reviews The American Society of Mechanical Engineers ATTN: R.E. White A.B. Wenzel 345 E. 47th Street New York, NY 10017
1	Atlantic Research Corp. ATTN: M.K. King 5390 Cherokee Avenue Alexandria, VA 22314
1	Atlantic Research Corp. ATTN: R.H.W. Waesche 7511 Wellington Road Gainesville, VA 22065
1	AVCO Everett Research Laboratory Division ATTN: D. Stickler 2385 Revere Beach Parkway Everett, MA 02149
1	Battelle Memorial Institute Tactical Technology Center ATTN: J. Huggins 505 King Avenue Columbus, OH 43201
1	Cohen Professional Services ATTN: N.S. Cohen 141 Channing Street Redlands, CA 92373
1	Exxon Research & Eng. Co. ATTN: A. Dean Route 22E Annandale, NJ 08801
1	Ford Aerospace and Communications Corp. DIVAD Division Div. Hq., Irvine ATTN: D. Williams Main Street & Ford Road Newport Beach, CA 92663
1	General Applied Science Laboratories, Inc. 77 Raynor Avenue Ronkonkoma, NY 11779-6649

<u>No. of Copies</u>	<u>Organization</u>
1	General Electric Ordnance Systems ATTN: J. Mandzy 100 Plastics Avenue Pittsfield, MA 01203
2	General Motors Rsch Labs Physics Department ATTN: T. Sloan R. Teets Warren, MI 48090
2	Hercules, Inc. Allegheny Ballistics Lab. ATTN: W.B. Walkup E.A. Yount P.O. Box 210 Rocket Center, WV 26726
1	Honeywell, Inc. Government and Aerospace Products ATTN: D.E. Broden/ MS MN50-2000 600 2nd Street NE Hopkins, MN 55343
1	Honeywell, Inc. ATTN: R.E. Tompkins MN38-3300 10400 Yellow Circle Drive Minnetonka, MN 55343
1	IBM Corporation ATTN: A.C. Tam Research Division 5600 Cottle Road San Jose, CA 95193
1	IIT Research Institute ATTN: R.F. Remaly 10 West 35th Street Chicago, IL 60616
2	Director Lawrence Livermore National Laboratory ATTN: C. Westbrook M. Costantino P.O. Box 808 Livermore, CA 94550
1	Lockheed Missiles & Space Co. ATTN: George Lo 3251 Hanover Street Dept. 52-35/B204/2 Palo Alto, CA 94304

<u>No. of Copies</u>	<u>Organization</u>
1	Los Alamos National Lab ATTN: B. Nichols T7, MS-B284 P.O. Box 1663 Los Alamos, NM 87545
1	National Science Foundation ATTN: A.B. Harvey Washington, DC 20550
1	Olin Ordnance ATTN: V. McDonald, Library P.O. Box 222 St. Marks, FL 32355-0222
1	Paul Gough Associates, Inc. ATTN: P.S. Gough 1048 South Street Portsmouth, NH 03801-5423
2	Princeton Combustion Research Laboratories, Inc. ATTN: M. Summerfield N.A. Messina 475 US Highway One Monmouth Junction, NJ 08852
1	Hughes Aircraft Company ATTN: T.E. Ward 8433 Fallbrook Avenue Canoga Park, CA 91303
1	Rockwell International Corp. Rocketdyne Division ATTN: J.E. Flanagan/HB02 6633 Canoga Avenue Canoga Park, CA 91304
4	Sandia National Laboratories Division 8354 ATTN: R. Cattolica S. Johnston P. Mattern D. Stephenson Livermore, CA 94550
1	Science Applications, Inc. ATTN: R.B. Edelman 23146 Cumorah Crest Woodland Hills, CA 91364
3	SRI International ATTN: G. Smith D. Crosley D. Golden 333 Ravenswood Avenue Menlo Park, CA 94025

<u>No. of Copies</u>	<u>Organization</u>
1	Stevens Institute of Tech. Davidson Laboratory ATTN: R. McAlevy, III Hoboken, NJ 07030
1	Thiokol Corporation Elkton Division ATTN: S.F. Palopoli P.O. Box 241 Elkton, MD 21921
1	Morton Thiokol, Inc. Huntsville Division ATTN: J. Deur Huntsville, AL 35807-7501
3	Thiokol Corporation Wasatch Division ATTN: S.J. Bennett P.O. Box 524 Brigham City, UT 84302
1	United Technologies Research Center ATTN: A.C. Eckbreth East Hartford, CT 06108
3	United Technologies Corp. Chemical Systems Division ATTN: R.S. Brown T.D. Myers (2 copies) P.O. Box 49028 San Jose, CA 95161-9028
1	Universal Propulsion Company ATTN: H.J. McSpadden Black Canyon Stage 1 Box 1140 Phoenix, AZ 85029
1	Veritay Technology, Inc. ATTN: E.B. Fisher 4845 Millersport Highway P.O. Box 305 East Amherst, NY 14051-0305
1	Brigham Young University Dept. of Chemical Engineering ATTN: M.W. Beckstead Provo, UT 84058
1	California Institute of Tech. Jet Propulsion Laboratory ATTN: L. Strand/MS 512/102 4800 Oak Grove Drive Pasadena, CA 91009

<u>No. of Copies</u>	<u>Organization</u>
1	California Institute of Technology ATTN: F.E.C. Culick/ MC 301-46 204 Karman Lab. Pasadena, CA 91125
1	University of California Los Alamos Scientific Lab. P.O. Box 1663, Mail Stop B216 Los Alamos, NM 87545
1	University of California, Berkeley Chemistry Department ATTN: C. Bradley Moore 211 Lewis Hall Berkeley, CA 94720
1	University of California, San Diego ATTN: F.A. Williams AMES, B010 La Jolla, CA 92093
2	University of California, Santa Barbara Quantum Institute ATTN: K. Schofield M. Steinberg Santa Barbara, CA 93106
1	University of Colorado at Boulder Engineering Center ATTN: J. Daily Campus Box 427 Boulder, CO 80309-0427
2	University of Southern California Dept. of Chemistry ATTN: S. Benson C. Wittig Los Angeles, CA 90007
1	Case Western Reserve Univ. Div. of Aerospace Sciences ATTN: J. Tien Cleveland, OH 44135
1	Cornell University Department of Chemistry ATTN: T.A. Cool Baker Laboratory Ithaca, NY 14853

<u>No. of Copies</u>	<u>Organization</u>
1	University of Delaware ATTN: T. Brill Chemistry Department Newark, DE 19711
1	University of Florida Dept. of Chemistry ATTN: J. Winefordner Gainesville, FL 32611
3	Georgia Institute of Technology School of Aerospace Engineering ATTN: E. Price W.C. Strahle B.T. Zinn Atlanta, GA 30332
1	University of Illinois Dept. of Mech. Eng. ATTN: H. Krier 144MEB, 1206 W. Green St. Urbana, IL 61801
1	Johns Hopkins University/APL Chemical Propulsion Information Agency ATTN: T.W. Christian Johns Hopkins Road Laurel, MD 20707
1	University of Michigan Gas Dynamics Lab Aerospace Engineering Bldg. ATTN: G.M. Faeth Ann Arbor, MI 48109-2140
1	University of Minnesota Dept. of Mechanical Engineering ATTN: E. Fletcher Minneapolis, MN 55455
3	Pennsylvania State University Applied Research Laboratory ATTN: K.K. Kuo H. Palmer M. Micci University Park, PA 16802
1	Pennsylvania State University Dept. of Mechanical Engineering ATTN: V. Yang University Park, PA 16802

<u>No. of Copies</u>	<u>Organization</u>
1	Polytechnic Institute of NY Graduate Center ATTN: S. Lederman Route 110 Farmingdale, NY 11735
2	Princeton University Forrestal Campus Library ATTN: K. Brezinsky I. Glassman P.O. Box 710 Princeton, NJ 08540
1	Purdue University School of Aeronautics and Astronautics ATTN: J.R. Osborn Grissom Hall West Lafayette, IN 47906
1	Purdue University Department of Chemistry ATTN: E. Grant West Lafayette, IN 47906
2	Purdue University School of Mechanical Engineering ATTN: N.M. Laurendeau S.N.B. Murthy TSPC Chaffee Hall West Lafayette, IN 47906
1	Rensselaer Polytechnic Inst. Dept. of Chemical Engineering ATTN: A. Fontijn Troy, NY 12181
1	Stanford University Dept. of Mechanical Engineering ATTN: R. Hanson Stanford, CA 94305
1	University of Texas Dept. of Chemistry ATTN: W. Gardiner Austin, TX 78712
1	University of Utah Dept. of Chemical Engineering ATTN: G. Flandro Salt Lake City, UT 84112

<u>No. of</u> <u>Copies</u>	<u>Organization</u>
1	Virginia Polytechnic Institute and State University ATTN: J.A. Schetz Blacksburg, VA 24061
1	Freedman Associates ATTN: E. Freedman 2411 Diana Road Baltimore, MD 21209-1525
2	Olin Corporation Ordnance Division ATTN: H. Mueller P.O. Box 21606 St. Petersburg, FL 21606
1	Honeywell, Inc. Armament Systems Division ATTN: B. Olsen Brooklyn Park, MN 55428
1	Armtec Defense Products, Inc. ATTN: H. Appleman Coachella, CA 92236

INTENTIONALLY LEFT BLANK

USE/ EVALUATION SHEET/CHANGE OF ADDRESS

This Laboratory undertakes a continuing effort to improve the quality of the reports it publishes. Your comments/answers to the items/questions below will aid us in our efforts.

1. BRL Report Number BRL-MR-3873 Date of Report OCTOBER 1990
2. Date Report Received _____
3. Does this report satisfy a need? (Comment on purpose, related project, or other area of interest for which the report will be used.) _____

4. Specifically, how is the report being used? (Information source, design data, procedure, source of ideas, etc.) _____

5. Has the information in this report led to any quantitative savings as far as man-hours or dollars saved, operating costs avoided, or efficiencies achieved, etc? If so, please elaborate. _____

6. General Comments. What do you think should be changed to improve future reports? (Indicate changes to organization, technical content, format, etc.) _____

CURRENT ADDRESS	_____
	Name

	Organization

	Address

	City, State, Zip Code

7. If indicating a Change of Address or Address Correction, please provide the New or Correct Address in Block 6 above and the Old or Incorrect address below.

OLD ADDRESS	_____
	Name

	Organization

	Address

	City, State, Zip Code

(Remove this sheet, fold as indicated, staple or tape closed, and mail.)

-----FOLD HERE-----

DEPARTMENT OF THE ARMY

Director
U.S. Army Ballistic Research Laboratory
ATTN: SLCBR-DD-T
Aberdeen Proving Ground, MD 21005-5066
OFFICIAL BUSINESS

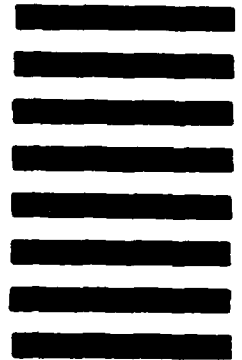


NO POSTAGE
NECESSARY
IF MAILED
IN THE
UNITED STATES

BUSINESS REPLY MAIL
FIRST CLASS PERMIT No 0001, APG, MD

POSTAGE WILL BE PAID BY ADDRESSEE

Director
U.S. Army Ballistic Research Laboratory
ATTN: SLCBR-DD-T
Aberdeen Proving Ground, MD 21005-9989



-----FOLD HERE-----